AALTO UNIVERSITY SCHOOL OF ENGINEERING

Department of Mechanics of Material

Strength and failure mechanism in 3D printed parts

Bishwonath Adhikari

Thesis submitted in partial fulfillment of the requirements for the degree of

Master of Science in Technology

Espoo

Supervisor: Professor Sven Bossyut

Instructor:

Aalto University
School of Engineering

Aalto University, P.O. BOX 11000, 00076
AALTO
www.aalto.fi

Abstract of master's thesis

Author Bishwonath Adhikari

Title of thesis Strength and Failure Mechanisms in 3D printed parts

Degree program Mechanical Engineering

Major Mechanics of Material **Code**

Thesis supervisor Prof. Sven Bossyut

Thesis advisor

Date 28.10.2016 **Number of pages** 80 pages **Language** English

Abstract

Additive Manufacturing, more commonly known as 3D printing is the way of quickly manufacturing the product, adding layer by layer, hence also known as rapid prototyping. Due to production time being very quick, it was mostly used for prototyping in the beginning. As, a result of more research and experiments, application area are increasing, and the process itself is being considered with high hopes for the future to replace some other complicated and traditional ways of production.

The major issue in the application of such product is the mechanical properties of the product that are dependent on too many building parameters. It is crucial to research on those parameters and the way those parameters affects individually to the strength properties of the end product. Also, the quantitative effect of the parameter on the end product is less known to say it clearly which parameters should be focused during production. Normally, strength properties of the parent material are lower in the end product and are too sensitive that the slight change in parameters, changes it significantly. Although the application areas of the 3D printed parts are rising, the research focused on prediction of the failure strength of such parts are not being carried out much. In these scenarios, use of such parts in the safety critical areas can be dangerous.

This research paper focuses on finding out if it is practical to use the already existing lamina theories in the strength prediction of the 3D printed parts as the strength of the 3D printed parts is also hugely affected by the layer orientation while 3D printing. Furthermore, wide varieties of test specimens used in mechanically loaded conditions are tested under loading conditions. The failure occurred during the experiment is later on analyzed using digital image correlation method and fracture surface analysis techniques.

Keywords 3D printing; Rapid prototyping; Strength Modeling; Failure Mechanism; DIC; Fracture Surface

Preface

This thesis is prepared for the completion of the Master's degree in mechanical engineering. This paper has been prepared for Aalto University, department of mechanics of material as a product of Master's degree study period.

This research would not have been possible without the direct and indirect contribution of few people. I would like to thank my thesis supervisor Professor Sven Bossyut for his valuable time and support throughout the entire process. Also, I would like to thank all my friends, helping and supporting me during my Master's study period. Master's study would not have been so smooth without their help.

Finally, I would like to appreciate the role of my family to make me stand at this point today. I am highly grateful for the motivation and support; they provide at each step of my life.

Contents

List of Figures

List of Tables

List of Graph

Abbreviations

ABS	Acrylonitrile Butadiene Styrene
PLA	Polylactic Acid
SLS	Selective Laser Sintering
FDM	Fused Deposition Modeling
3D	Three Dimensional
CAD	Computer Aided Design
CAE	Computer Aided Engineering
Max. Stress	Maximum Stress
STL	Stereolithography
PA	Poly Amide
ISO	International Organization for Standardization
ASTM	American Society for Testing and Materials
DIC	Digital Image Correlation
CCD	Charged Coupled Device
FEA	Finite Element Analysis
LSM	Least Square Image Matching

Introduction

3D printing has become easily accessible even for the domestic users. Thus, 3D printed parts are on the rise to be used in different application field. Though the use of 3D printed parts has increased significantly, strength calculation and failure prediction in such parts have not advanced so much. There is not any certified or widely accepted way to calculate the strength of such parts accurately. Much work has not been done to provide the answer whether 3D printed parts should be treated in the material level or structural level. 3D printed parts appears as the single unit as an end product similar to that of composite materials. Composite materials can be treated as a material and use the lamina theories for the strength calculation and failure prediction. This research focuses on finding out first whether 3D printed material can use the same principle to predict its failure or the 3D printed materials should be treated as structure although the end product is one single unit. First, the theoretical analysis is done to find if there is any feasible failure theory that already exists. Layer orientation in the 3D printing plays a significant part in determining the strength of the 3D printed parts as in the case of composite materials. Lamina theories are considered in the beginning to be the close fit for the strength calculation of 3D printed materials for theoretical analysis. [1, 2, and 4] After that, 3D printed test specimen is experimented to verify the strength of 3D printed parts according to the outcome of the theoretical analysis. Experimental test specimen will be discussed in the later part of the research.

1.1 Additive Manufacturing

Additive Manufacturing, commonly known as rapid prototyping is the way of manufacturing the product, adding layers on top of preceding layer. Due to production process being uncomplicated, it was mostly used for prototyping in the beginning. As a result of more research and experiments, application areas are increasing, and the process is considered with high hopes for the future to replace some other complicated and traditional ways of production. As explained by the term additive manufacturing, products are produced, adding the material layer by layer. One layer is deposited on top on another which allows manufacturing the complicated shapes that are difficult to manufacture by alternative way. It eliminates the requirement of using expensive tooling and machining process. Compared to the material removal approach to manufacturing the products, additive manufacturing is usually easier to manufacture the complex shaped

materials. Also, the additive manufacturing process uses less material compared to the material removal process. The waste generated in material removal approach is high but almost none in additive manufacturing. Products made from plastic materials like ABS and PLA are cheap enough for domestic production and also the building equipment are less expensive and easily available. Additive manufacturing using metals as the material is also possible but are slightly expensive which is mostly limited to industrial and research purposes.

The additive manufacturing process has already made some progress in increasing its application area. More researches are being focused in different areas of additive manufacturing for example production technology, strength modeling. Different technologies of additive manufacturing are in use today, and few popular examples are 3D printing, Stereolithography, SLS, FDM. This research project mostly covers 3D printing.

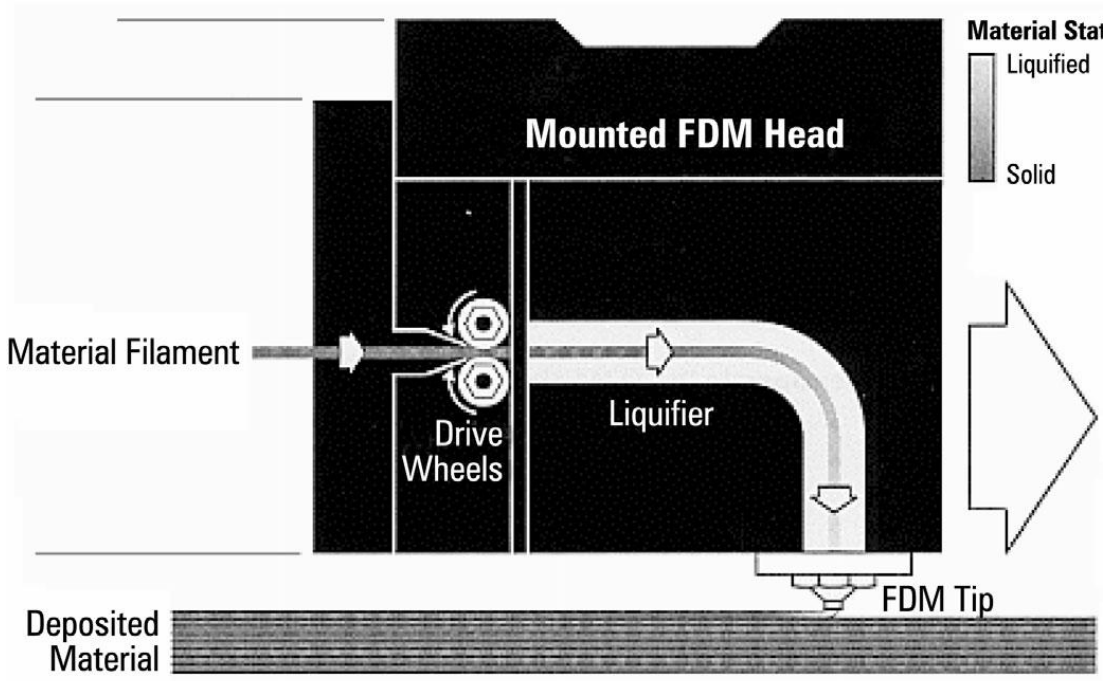

Figure 1: FDM Process [1]

1.2 Manufacturing Process

The additive manufacturing process has two main sub-processes.

- CAD
- 3D-printing

CAD and 3D-printing have together added a new dimension to manufacturing objects. The manufacturing process starts first with the creation of the object virtually in a computer with the aid of the CAD software that is present in numbers these days or by scanning components physically. STL format is created from designed 3D model that contains information about the object by meshing into smaller triangular pieces. The whole object now according to the STL format looks like built of small triangular bricks. STL file is exported to the Quickslice software where the object is dissected horizontally into many thin sections into a series of thickness planes. This data is exported to the 3D printer. The minimum thickness of the layer depends upon the capability of the printer to produce the thinnest layer from its nozzle. The increase in thickness normally means the decrease in printing time, but it degrades the quality of end product on both strength and surface finish. Layer thickness is defined at this stage. Then starts the deposition of the molten material layer by layer horizontally and finally creates the part at the end.

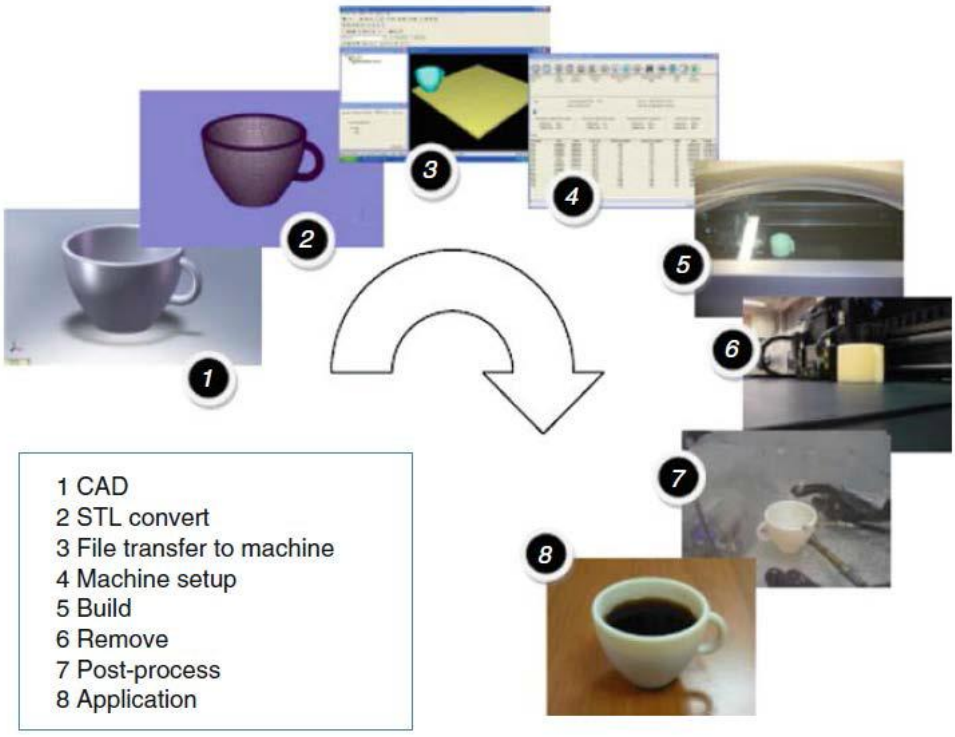

Figure 2: Stages involved in additive manufacturing [2]

1.3 Objectives

The availability of the 3D printers has become so common that application of 3D printed parts is in a rise in different fields. However, significant work is not done yet to predict the strength and failure mechanisms accurately in the 3D printed parts. In fact, the strength of the 3D printed parts depends on so many parameters that it is not easier to calculate accurately, when and how the failure in such parts is going to happen. It is not likely that such equation will be modeled soon that includes all the parameters that affect the strength of the 3D printed parts. On the other hand, use of such printed parts as a load carrying component in the machines has already deep rooted. The aim of the research is to analyze the failure theories used to calculate the failure in composite structures and to find if they are feasible to calculate accurately the strength of 3D printed parts.

Another, objective of the research is to perform the experimentation of strength of 3D printed parts with different test specimen compared to other previous research that mostly used dog bone structure to test according to the standard ASTM D368. There is not any standard test specimen defined yet to test the strength of 3D printed parts. The standard used in previous research followed the same standard that is used for testing other isotropic plastic material strength. Often the researchers are facing challenges to test the sample accurately due to premature failure in 3D printed parts. This research is also aimed to experiment different type of 3D printed parts than used before which might contribute defining the standard test specimen in future.

1.4 Research Method

There are two major parts in this research work:

Theoretical Part

Experiment/Observation

In the theoretical part, the basic concept of additive manufacturing and its process, building parameters and its effects on mechanical properties are introduced. Previous researches on the mechanical properties of the 3D printed parts are reviewed in this section. The theoretical part is based on research scientific articles and textbooks. Due to the lack of enough research, it has always been confusing if the 3D printed parts can be treated as material or structure. No research work is done to validate how accurate the strength prediction of the 3D printed things can be done considering the 3D printed parts as material, using the already present failure theories that are used to calculate the

failure in anisotropic materials. So, this research starts from the point trying to validate if those theories work for 3D printed parts as material or not. This section of the research gives the idea to proceed forward and analyze the strength and failures of the 3D printed parts as material or structure.

In the experimental part of the thesis, different types of 3D printed parts are manufactured using the 3D printing technology that can be loaded mechanically. There is not any standard test specimen for 3D printed parts yet. So, the various parts that are being used or can be used in real life are tested to cover the vast area of failures that happens in 3D printed products. Experiments are carried out with printed specimens using the various loads. The failures occurred on the specimen are observed and analyzed using digital image correlation (DIC).

2 Literature Review

Much research in mechanical properties of 3D printed parts is done before. Most of the research are based on the experimental approach and comparing the failure of the same material, varying the parameters that affect the strength. Most of the experiment used the similar kind of shape manufactured using some standard for example ASTM or ISO standard. As stated in ref [2], according to ASTM D638-10 standard, FDM modeled test specimen is treated as beams. Breadth and height of the specimen are comparatively very small to length. When a tensile load is applied in the lengthwise direction, deformation will be uniform with distributed strain. The popular shape in most of such type of experiment is bone shaped printed parts as shown in the figure below.

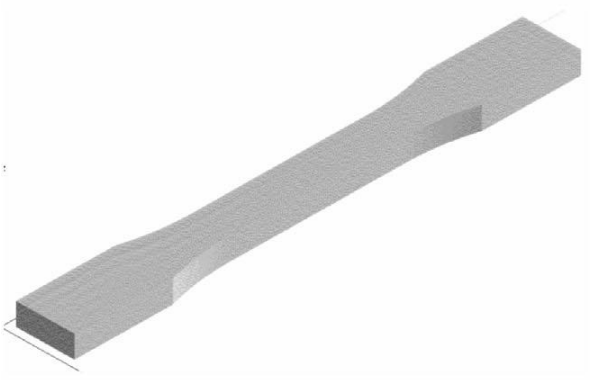

Figure 3: Most popular experimental test specimen

Almost all the previous research showed that the 3D printed parts are anisotropic by nature i.e. they exhibit different strength in a different direction. The raster orientation defines the direction, and the strengths are different parallel to it and perpendicular to it. The strength of the part is highest when the raster orientation is parallel to the loading direction and it starts to decrease as the raster angle increases. Minimum stress value is attained when the raster angle is 90 degrees [5].According to the ref. [1], test specimen tested according to ASTM D638 standard resulted in the premature failure. The premature failure moreover looks like because of the test specimen shape and building ways rather than the testing standard. So the testing standard followed in ref [1] is changed from ASTM D638 to ASTM D3039 which still does not guarantee that the same failure will not occur as specimen used was same. Only loading condition was different. Not only the build directions but few other parameters also affect the strength of the 3D printed parts. Research focused towards formulating the equation which predicts the failure of 3D printed parts and considers all the parameters that affect the strength, is not done before.

2.1 Effects of build parameters

Objects are created by depositing line by line and layer by layer. Built direction and the compactness of the material and few other factors affect the strength of the object in considerable amount. Normally, strength properties of the parent material are lower in the end product and are too sensitive that the slight change in parameters, changes it dramatically. Some of the parameters that affect the properties mechanically are discussed below. [1, 3, 5]

2.1.1 Bead width

It is the thickness of the material that comes out of the printer. Its size can be varied but cannot be less than the threshold capability of the printing machine to print a layer. Melted material comes out of the tip of the printer as ink comes out of the tip of a pen. It is highly viscous so always comes out with the constant thickness and that thickness is called bead width. [3] Bead width directly affects the compactness of the layer in the end product altering the material properties. The larger thickness of the bead means more possibility of pores in the end product which obviously affects the strength, but ref [1] found that the bead width is of less significance compared to other parameters.

2.1.2 Layer Orientation

3D printed parts are built layer by layer. So, building angle of the layer deposition affects the mechanical properties hugely which make the object anisotropic/orthotropic. The angle between the applied force and built direction determine the component of the forces that acts on the object. Even though the force acts in one principal axis, due to the raster orientation the force might affect the object in another principal axis [3]. Due to the layer bonding effect of the force splits into material orientation and normal to it. [5]

2.1.3 Air Gap

It is the gap between two adjacent rasters which can be positive or negative. Positive means the gap is present and negative means they are overlapped. This factor also causes the compactness of the material in the product resulting, varying mechanical properties. [3]

2.1.4 Contours

The number of contours and also the way it is contoured decides the mechanical properties. Contours play a direct role in creating the stress concentration points which are vital regarding the strength of the object. [5] According to ref [2] counters play a noticeable role in strengthening the mechanical properties compared to not having it in possible places.

2.1.5 Build temperature

It determines the viscosity of molten material which after solidifying affect the density of the material and also the thickness of the material which eventually affects the strength of the object. [3]

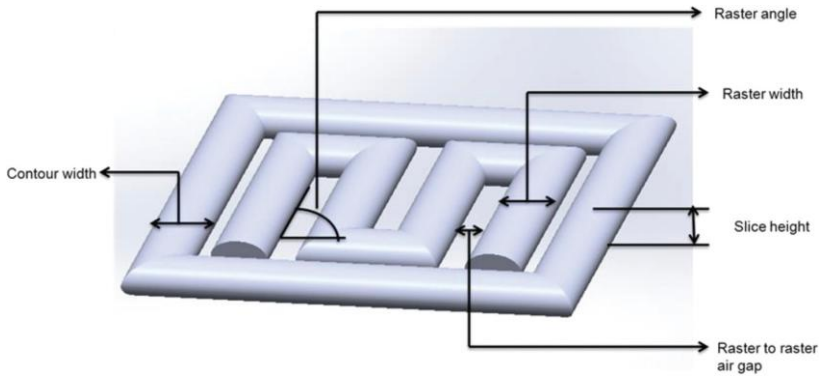

Figure 4: Building Parameters [5]

2.2 Material Properties

The basic idea of manufacturing 3-D printed materials involves creating the object by printing layer by layer. So, 3-D printed objects can be defined as the stack of the material layers of which each layer is called as a lamina. Based on the manufacturing technique, a new coordinate system can be defined as a 1-2-Z coordinate system of which parallel to layer oriented direction is 1-axis, orthogonal to the layer oriented 1-axis is 2-axis and the lamina deposited direction is Z direction. Many experiments were done in the past to study the mechanical behaviors of 3-D printed materials. This lead to the fact that 3-D printed materials behaves orthotropically similar to the composite laminates. They have different strength property in different principal material axes. The following symbols are used in this paper to define the respective strengths in different principal axes.

X_t: tensile strength in 1-axis

Y_t: tensile strength in 2-axis

X_c: compressive strength in 1-axis

Y_c: compressive strength in 2-axis

S: shear strength

The strength of the material used for 3D printing may vary from the parent material as it undergoes melting and solidification. Also the layer deposition parameter, for example, the layer gap, bead size determines it strength. It is important to define the strength of the material after the printing is done to get the precise prediction of the failure in 3D printed parts.

Many theories that explain the failure criterion exists which are used to predict the failure of the isotropic material. These theories use the material properties determined by the uniaxial tensile, compressive and shear tests. The same approach can be used to find out the material properties. Firstly, through the uniaxial tensile, compressive and shear tests, material properties can be defined in both material direction and the perpendicular direction to it.

X_t is determined, applying the uniaxial tensile stress test to the specimens with only 0° layer orientation i.e. the stress and layer orientation have the same direction Y_t is determined by applying uniaxial tensile stress test with only 90° layer orientation i.e. the stress direction is perpendicular to the layer orientation. In the same way, compressive strength magnitude in both 1-axis and 2-axis is determined by applying a uniaxial compressive stress test to the 0° and 90° layer orientated specimen respectively. These

determined strength values can be used as the threshold values in the respective direction to calculate the strength of the parts under all combination of stress components in different directions. The magnitude of ultimate tensile stress and ultimate compressive stress are different in the case of composite structures but same in the case of metals, plastic and other brittle materials too. Now failure theories can be used to predict the failure using those material properties. However, to predict the failure of 3D printed parts, the applied stresses must be transformed in the material direction and perpendicular to it as shown in equation 1 below. [1, 6]

2.3 Failure Criteria

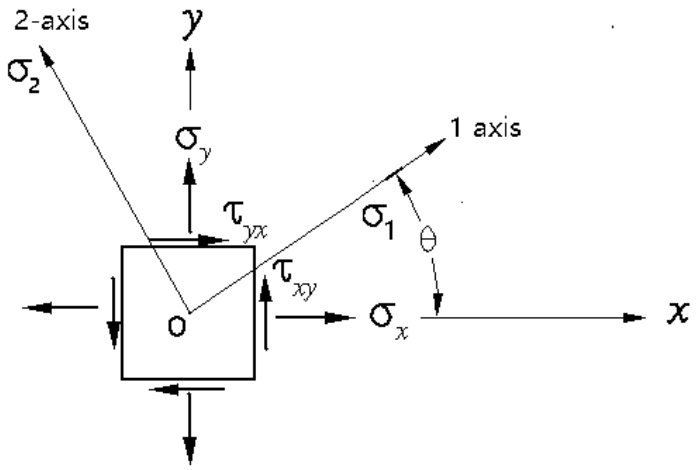

Figure 5: Body under all stress condition

Let's suppose the coordinate system as illustrated in the figure above. Where,

X and Y are the main axes,

σ_x: Stress in X-axis

σ_y : Stress in Y-axis

$\tau_{xy} = \tau_{yx}$: Shear stress components

1-axis: Hypothetical axis parallel to material layer oriented direction

2-axis: hypothetical axis perpendicular to material layer oriented direction

Θ: angle between the X-axis and 1-axis or between two co-ordinate systems

σ_1: Stress in 1 direction due to σ_x, σ_y and τ_{xy}

σ_2: Stress in 2 direction due to σ_x,σ_y and τ_{xy}

$\tau_{12} = \tau_{21}$: Shear stress in 2 direction due to σ_x,σ_y and τ_{xy}

As the threshold values of stresses in 3D printed parts is only known in material direction, only possible way to calculate the failure criterion is to transform all the stress components to the principal material axes.

Transforming σ_x,σ_y andτ_{xy} in to the 1-2 co-ordinate axis we get,

$$\sigma_1 = \sigma_x cos^2\theta + \sigma_y sin^2\theta + 2\tau_{xy} cos\theta sin\theta$$
$$\sigma_2 = \sigma_x sin^2\theta + \sigma_y cos^2\theta - 2\tau_{xy} cos\theta sin\theta \quad \text{…Eq.1}$$
$$\tau_{12} = (\sigma_x - \sigma_y) cos\theta\, sin\theta + \tau_{xy}(cos^2\theta - sin^2\theta)$$

For the simplicity of the problem and to make it easier to understand, strength test experiments are usually done in uniaxial stress condition, i.e. the stress in the experimenting body applied in only one direction. In this case, following uniaxial case is considered.

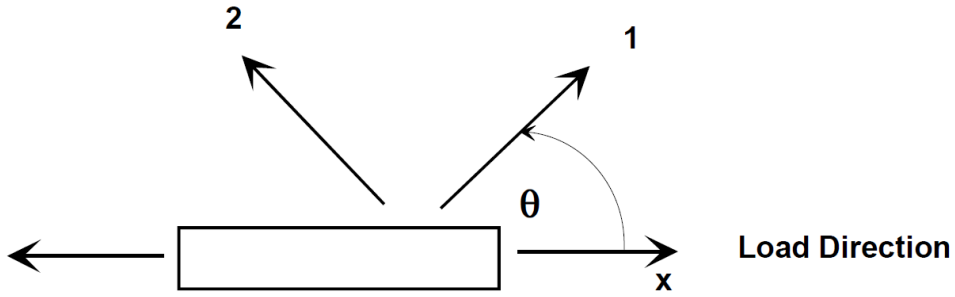

Figure 6 Body under uniaxial stress

Only, stress in the x-direction is applied of the magnitude σ, which has the following effect on the layer direction and perpendicular direction to it.

$$\sigma_1 = \sigma \cos^2\theta$$
$$\sigma_2 = \sigma \sin^2\theta \quad \text{…Eq. 2}$$
$$\tau_{12} = -\sigma cos\theta sin\theta$$

Although many failure criteria are in use today, few of the mostly used criteria with their condition are explained below. All these criteria are possible to define from generalized form into uniaxial stress form. Uniaxial stress forms are easier to compare with each other to find out the best possible failure criteria for the 3D printed materials.

2.3.1 Maximum Stress Criteria

General form of the equation of maximum stress criteria:

$$\left|\frac{\sigma_1}{X}\right|, \left|\frac{\sigma_2}{Y}\right|, \left|\frac{\tau_{12}}{S}\right| \geq 1 \qquad \text{...Eq.3}$$

Where,

X = X_c if $\sigma_1 < 0$

X = X_t if $\sigma_1 \geq 0$

Y = Y_c if $\sigma_2 < 0$

Y = Y_t if $\sigma_2 \geq 0$

All three cases explained in equation 2 must satisfy in any case to keep the stressed material without failure. Violation of any one of them or two or all causes the failure in the material.

According to maximum stress criteria, Failure occurs when one of the inequalities is satisfied either $\left|\frac{\sigma_1}{X}\right| \geq 1$or $\left|\frac{\sigma_2}{Y}\right| \geq 1or\left|\frac{\tau_{12}}{S}\right| \geq 1$. Although equation includes all three strength factor i.e. X, Y and S, but there is no interaction between one another. Generally when the failure occurs, only one of those values is responsible for the failure. X, Y and S, acts as threshold value for each components of the stress. For example X acts as threshold value for stress component in material oriented direction, Y acts as threshold value for stress component in direction perpendicular to material oriented direction and S acts as the threshold value for shear stress component. One stress component never affects the other two threshold values except the one in its direction. For instance stress component in material oriented direction is never affected by Y or S value. This applies to all stress component that the other two threshold values never affects that stress component. This failure criterion is normally feasible to those types of material which has same magnitude of tensile strength and compressive strength. [22] The failure envelope is rectangular in the stress space which is formed from the intersecting straight lines. [26]

For the uniaxial stress case, from equation 2 and 3, we get,

$$\sigma = \left|\frac{X}{\cos^2\theta}\right| \text{ Or } \left|\frac{Y}{\sin^2\theta}\right| \text{ Or } \left|\frac{S}{cos\theta sin\theta}\right| \qquad \text{…Eq. 4[7]}$$

2.3.2 Tsai-Hill Criteria

This theory is proposed as the generalized form of Von Mises-Hencky maximum distortional energy theory to work for anisotropic materials. Unlike Maximum stress criteria, this theory considers the interaction of different failure strength to produce smooth failure envelope. This theory though does not consider different strengths for tensile and compressive strength. Both tensile strength and compressive strength of the

material must be same which can be regarded as a demerit of this theory. Also, the failure strength cannot be predicted, but the only onset to the failure can be predicted using this theory. [26]

General formulation of the Tsai-Hill Criteria,

$$\frac{\sigma_1^2}{X^2} + \frac{\sigma_2^2}{Y^2} - \frac{\sigma_1\sigma_2}{X^2} + \frac{\tau_{12}^2}{S^2} = 1 \quad \text{…Eq. 5}$$

Where,

$X = X_c$ if $\sigma_1 < 0$

$X = X_t$ if $\sigma_1 \geq 0$

$Y = Y_c$ if $\sigma_2 < 0$

$Y = Y_t$ if $\sigma_2 \geq 0$

X and Y are strengths in x, and y-direction respectively which can be substituted by tensile strength and compressive strength depending upon the condition and S is the shear strength. However, in the case of 3D printed parts strength in both directions is considered of the same magnitude as in metals and other brittle materials.

Now, using equation 3 and 4 to derive the uniaxial case for Tsai-Hill criteria, we get-

$$\sigma^2 = \frac{1}{\frac{\cos^4\theta}{X^2} + \frac{\sin^4\theta}{Y^2} + \cos^2\theta\sin^2\theta\left(\frac{1}{S^2} - \frac{1}{X^2}\right)} \quad \text{…Eq. 6[7]}$$

2.3.3 Hoffman Criteria

Hoffman criterion is a generalized form of Tsai-Hill criteria for different tensile and compressive failure strength. Once the compressive and tensile failure stress is replaced with the same identity, this criterion reduces exactly same as Tsai-Hill criteria. So, there is nothing new in this criterion compared to Tsai-Hill criterion as both compressive and tensile failure stress is considered to be same for 3D printed materials, in this research. [26]

General form of Hoffman's equation:

$$1 = \frac{\sigma_1^2}{X_t X_c} + \frac{\sigma_2^2}{Y_t Y_c} + \frac{\tau_{12}^2}{S^2} + \left(\frac{1}{X_t} - \frac{1}{X_c}\right)\sigma_1 + \left(\frac{1}{Y_t} - \frac{1}{Y_c}\right)\sigma_2 - \frac{\sigma_1\sigma_2}{X_t X_c} \quad \text{…Eq. 7}$$

Hoffman Criteria considers both compression and tension in the same equation. As discussed in limitations, using the same magnitude value for compressive and tensile strength of the 3D printed material as in metals or other brittle materials, we get-

$$1 = \frac{\sigma_1^2}{X^2} + \frac{\sigma_2^2}{Y^2} + \frac{\tau_{12}^2}{S^2} - \frac{\sigma_1\sigma_2}{X^2} \qquad \text{…Eq. 8}$$

Now, using equation 2 and 8 to find the critical uniaxial tensile stress, we get-

$$\sigma^2 \left\{ \frac{\cos^4\theta}{X^2} + \frac{\sin^4\theta}{Y^2} + \cos^2\theta \sin^2\theta \left(\frac{1}{S^2} - \frac{1}{X^2} \right) \right\} = 1 \qquad \text{…Eq. 9}$$

Comparing the Hoffman criteria and Tsai-Hill criteria shows that both the criteria reduce to the same equation in the case of the uniaxial testing condition of the material which has the same magnitude of both tensile and compressive strength. [7]

2.3.4 Norris and McKinnon

This theory is also the generalized form of Von Mises-Hencky maximum distortional energy theory as Tsai-Hill criterion. There is a slight difference between these two theories which makes this theory stand out as the best fit theory for the fatigue test results. [26]

Norris and McKinnon's criteria state that;

$$\frac{\sigma_1^2}{X^2} + \frac{\sigma_2^2}{Y^2} + \frac{\tau_{12}}{S^2} = 1 \qquad \text{…Eq. 10}$$

Similar to Tsai-Hill Criteria,

$X = X_c$ if $\sigma_1 < 0$

$X = X_t$ if $\sigma_1 \geq 0$

$Y = Y_c$ if $\sigma_2 < 0$

$Y = Y_t$ if $\sigma_2 \geq 0$

Changing the above relation into uniaxial stress case and finding the critical magnitudes of uniaxial stress gives the following condition.

$$\sigma^2 = \frac{1}{\frac{\cos^4\theta}{X^2} + \frac{\sin^4\theta}{Y^2} + \frac{\cos^2\theta \sin^2\theta}{S^2}} \text{…Eq. 11[7]}$$

2.3.5 Tsai-Wu Criterion

This theory also put emphasis on different tensile and compressive failure stress similar to Hoffman criteria. Different research has validated this theory as one of the most accurate formulations for engineering application. However, this theory has not been applied much as it is hard to determine the strength tensors form used in this criterion. [26]

General form of Tsai-Wu criteria can be stated as:

$$\left(\frac{1}{X_t}-\frac{1}{X_c}\right)\sigma_1+\left(\frac{1}{Y_t}-\frac{1}{Y_c}\right)\sigma_2+\frac{\sigma_1^2}{X_t*X_c}+\frac{\sigma_2^2}{Y_t*Y_c}-\frac{1}{2}*\sqrt{\frac{1}{X_tX_cY_tY_c}}\sigma_1*\sigma_2+\frac{\tau_{12}^2}{S^2}=1 \ldots\text{Eq. 12}$$

After using $X_t=X_c=X, Y_t=Y_c=Y$ we get,

$$\frac{\sigma_1^2}{X^2}+\frac{\sigma_2^2}{Y^2}-\frac{1}{2}*\sqrt{\frac{1}{X^2Y^2}}\sigma_1*\sigma_2+\frac{\tau_{12}^2}{S^2}=1 \quad \ldots\text{Eq. 13}$$

Finding the critical uniaxial stress value using equation 2 and 12 we get-

$$\sigma^2\left\{\frac{\cos^4\theta}{X^2}+\frac{\sin^4\theta}{Y^2}+\frac{1}{2}*\cos^2\theta\sin^2\theta\left(\frac{1}{S^2}-\frac{1}{XY}\right)\right\}=1 \quad \text{Eq. 14[7]}$$

2.3.6 Malmeister Criterion

Malmeister generalized the Ashkenazi theory which is now known as Malmeister criterion. Ashkenazi theory is complicated strength criterion for highly anisotropic material if the plane state of stress for such material is considered. The coefficient used in the criteria is required to be determined from the experimental data for biaxial states of stress. [26]

Similarly, the equation for Malmeister criterion is as follows:

$$\frac{\sigma_1^2}{X_tX_c}+\frac{\sigma_2^2}{Y_tY_c}+\frac{\tau_{12}^2}{S^2}+\left(\frac{1}{X_t}-\frac{1}{X_c}\right)\sigma_1+\left(\frac{1}{Y_T}-\frac{1}{Y_c}\right)\sigma_2+\left(\frac{1}{X_tX_c}-\left(\frac{X_tX_c-S\{X_c-X_t-X_c\left(\frac{X_t}{Y_t}\right)+Y\}}{2S^2X_tX_c}\right)\right)\sigma_1\sigma_2=1 \ldots\text{Eq. 15}$$

Similarly, using the same tensile and compressive strength we get-

$$\frac{\sigma_1^2}{X^2}+\frac{\sigma_2^2}{Y^2}+\frac{\tau_{12}^2}{S^2}+\left(\left(\frac{2S^2-X^2-SX\left(\frac{X}{Y}\right)-SY}{2S^2X^2}\right)\right)\sigma_1\sigma_2=1$$

According to the uniaxial test condition and Malmeister criterion, critical uniaxial stress is given by;

$$\sigma^2\left\{\frac{\cos^4\theta}{X^2}+\frac{\sin^4\theta}{Y^2}+\cos^2\theta\sin^2\theta\left(\frac{1}{S^2}+\frac{2S^2-X^2-SX\left(\frac{X}{Y}\right)-SY}{2S^2X^2}\right)\right\}=1\ldots\ldots\text{Eq. 16 [7]}$$

2.3.7 Failure criteria Conclusion

Some conclusions can be drawn after studying different types of failure criteria. The failure stress at 0 degrees and 90 degrees are material properties which are always constant for one material for all failure criteria which are determined by the experimental tests. All the failure criteria define the failure stress between 0 and 90 degrees according to their formulation. Failure stresses calculated by two different failure criteria can be different although the angle and material properties are same. All the failure criteria define its route of degrading failure stress from 0 degrees to 90 degrees with increasing angle.

2.4 Theoretical Results

One of the material properties is still unknown in the failure criteria formulations i.e. shear strength ‘S’ value. The magnitude of S is varied according to the linear relation with the failure stress of the material at 0 degrees. ‘S’ value has been varied because there is not enough research done to determine the value of ‘S.' Most of the researches have been done to determine only ‘X’ and ‘Y.' Ultimate shear strength is stated in the manufacturer’s data sheet from which it is found that the magnitude of ‘S’ in the case of 3D printed parts are approximately 1.5. This value will be used later on to compare the ‘S’ value found from the comparison of the experimental result and theoretical result.

Three cases are fixed as defined below. One case is varied to check and determine the value of ‘S’ where the experimental result and the theoretical result come close to each other. Failure stress is calculated for all four cases below for all the data sets.

When,

$S = 0.1*X$

$S = 0.4/0.5* X$

$S = 1* X$

Where,

X = Tensile strength in material oriented direction

S = Shear strength

Above three cases are considered to calculate the critical failure stress at a different angle of layer orientation and plotted on the same graph. The fourth case is determined analyzing the first three cases and the experimental result. The values of ‘S’ is adjusted analyzing the first three cases so that the theoretical result is closer to experimental result. The process is repeated for five different failure criteria explained above except the

Hoffman criteria. Hoffman criteria and Tsai-Hill criteria have the same expression for the uniaxial critical failure stress. Total of eleven values for each angle orientation i.e. 0, 30, 60, and 90 are obtained for each of above four cases. X-axis represents the angle whereas Y-axis represents the ratio between the ultimate strength of the material to the failure stress of the material at the given angle. Ultimate strength used in the ratio is the tensile failure strength when the layer build direction is parallel to the load direction. Four different graph lines are produced depending on the value of shear strength 'S.'

Table 1 Collected Datasheets

Number	Material	X	Y	Reference
1	Vero Blue	49,7	18,5	Aalto Lab
2	ABS PLUS	31,8	11,2	Aalto Lab
3	ABS	21	9,3	[9]
4	ABS P400	22	12	[1]
5	ABS	24	13	[10]
6	ABS	28,4	14,3	[11]
7	ABS 5% JUTE	25,9	9,1	[11]
8	ABS 5% TIO2	32,2	18,4	[11]
9	ABS 5% TPE	24	12,9	[11]
10	PA	30	15	[13]
11	ABS	25,72	14,56	[12]

The table above consist data collected from different previously published research papers. These data sets are used to calculate the failure stress in the uniaxial stress test condition using the equation derived for different failure criteria above. Each pair of dataset is used to calculate the critical uniaxial failure stress for five different failure criteria

From the table, it can be noticed that the materials are not same for all the collected data sets so the failure stress cannot be compared or combined directly. Instead, the ratio of the failure stress calculated at different raster angle orientation to its maximum stress i.e. stress at angle 0-degree raster orientation is compared. It is obvious from the different previous research that the tensile strength is highest when the build angle of the layer is 0 degrees. So, the calculated failure stress at each angle is divided by the tensile failure stress at 0 degrees of itself. That produces the ratio of two stresses which shows the proportion by which the failure strength is degrading compared to the failure

stress at 0 degrees. Both experimental and theoretical results are calculated in a similar way so that it would be easier to obtain the average result and to compare the theoretical result and experimental result. An example is explained here to make the method easy to understand. Firstly, from the table, data set 1 is taken. These values of X= 49.7 and Y = 18.5 are used to calculate the failure stress at 0, 30, 60, 90 degrees. Each failure stress is divided by the X = 49.7 to get the ratio by which its failure strength decreases with increasing angle and plotted in the graph. Similarly, for the data set 2, X = 31.8 and Y = 11.2 is taken and are used to calculate the failure stress at 0, 30, 60 and 90 degrees. Those failure stress are divided by the X = 31.8, and the degrading ratio of failure strength with increasing angle is obtained, and those ratios are plotted in the graph. The process is repeated for all the collected data and plotted in the same graph for each failure criteria.

2.4.1 Maximum Stress Criteria

Maximum stress criteria as stated in Equation 3, is used to calculate the failure stress for different angles of material layer orientation and creating a plot as explained above produced the following result and graph.

Table 2 Summary of Max Stress criteria

S. No	S -Value	Ratio Range (σ/X)			
		Angle			
		0	30	60	90
1	0,1*X	1	0,23	0,23	0,35-0,57
2	0,4*X	1	0,92	0,47-0,76	0,35-0,57
3	0,5*X	1	1,15	0,47-0,76	0,35-0,57
4	1*X	1	1,33	0,47-0,76	0,35-0,57

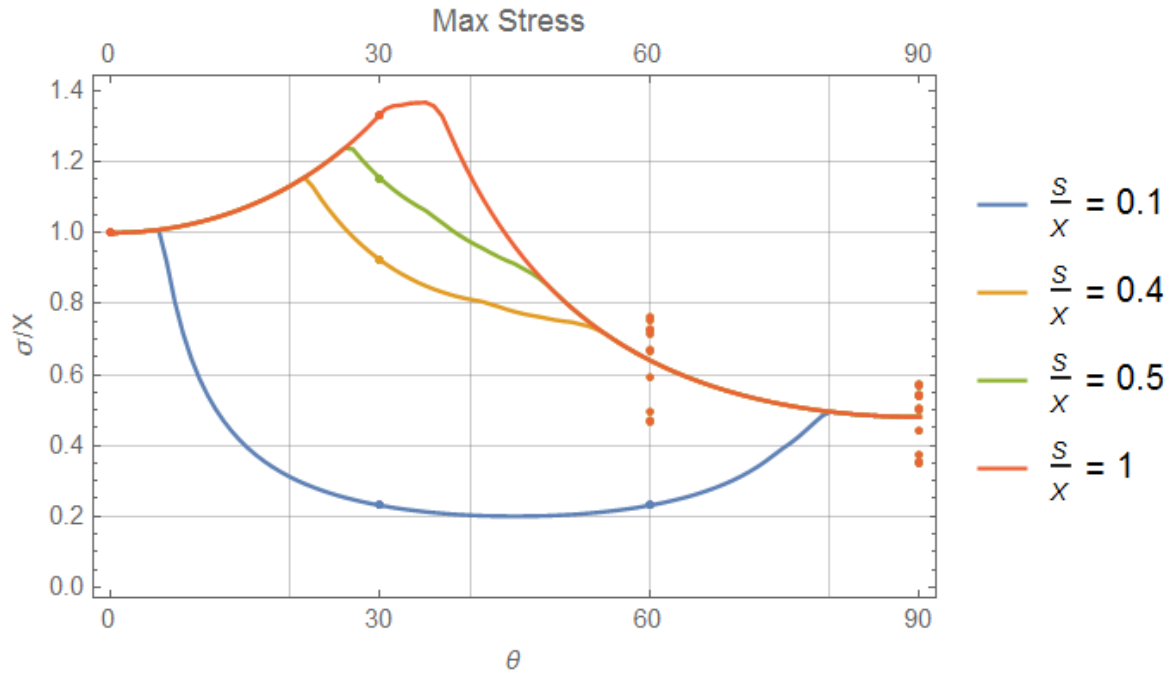

Graph 1 Graphical Presentation Max. Stress Result

Firstly, the four previously stated condition of S- value is used to calculate the data required for plotting at different angles. When the ultimate shear stress strength is relatively very low i.e. S=0.1*X, failure stress decreased rapidly until 30 degrees, then remains constant until 60 degrees. It started to increase linearly until the ratio of failure stress to ultimate stress reached 0.5. Slope changes after it reaches 0.5 on the way to 90 degrees. For S=0.4*X, the failure stress began to increase with low slope value with increasing angle, until the angle hits approximately 20-25 degrees. Then the slope decreased slightly, and failure stress continued to decline with that slope value until 90 with a negligible change of slope value at 60 degrees. For case 3 and 4, failure stress started to increase in magnitude until the value is approximately 30 degrees.

2.4.2 Tsai-Hill Criteria

Table 3 Summary of Tsai-Hill Criteria Result

S. No	S -Value	Ratio range (σ/X)			
		Angle			
		0	30	60	90
1	0,1*X	1	0,23	0,21-0,22	0,35-0,57
2	0,4*X	1	0,70-0,76	0,42-0,60	0,35-0,57
3	0,55*X	1	0,82-0,92	0,44-0,67	0,35-0,57
4	1*X	1	0,97-1,15	0,47-0,74	0,35-0,57

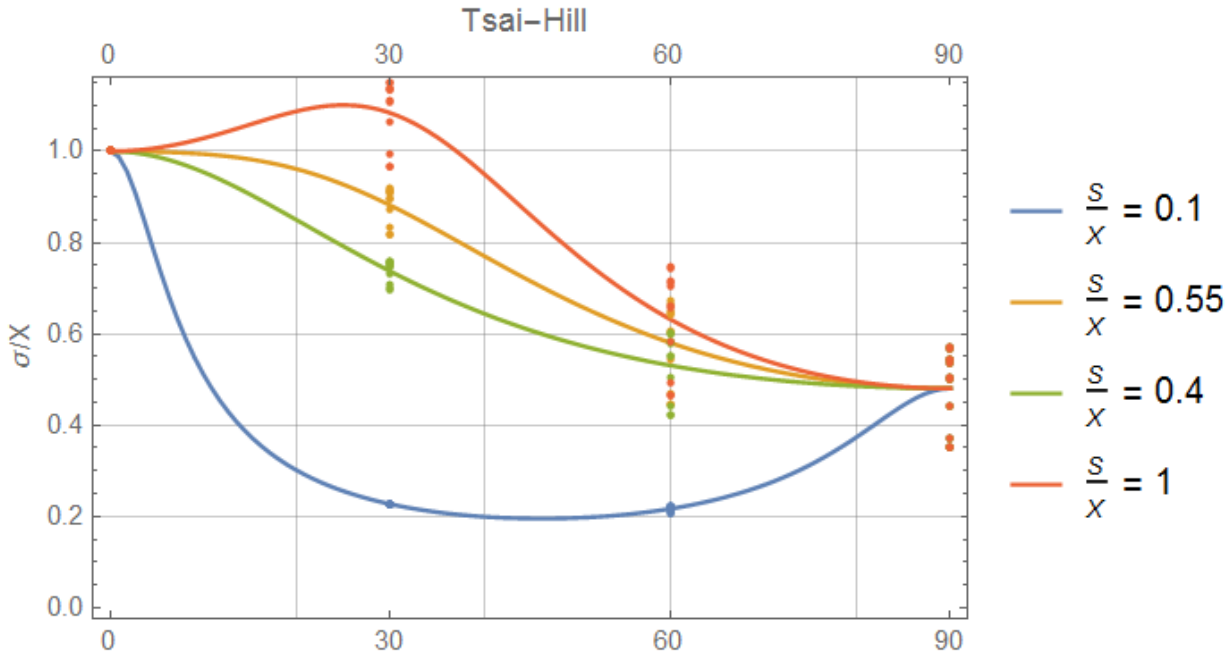

Graph 2 Graphical Presentation Tsai-Hill Result

The graph is plotted according to the Tsai-Hill criteria, for all 4 values of shear strength, using all the sets of data collected. The result of the plotting can be seen above with four distinct lines for four different approximate values of shear strength. In the first case, when the value of S is 0.1, failure stress value started to decrease dramatically in the beginning with the increasing angle until 30 degrees. Failure stress remained constant for next 30 degrees and began to increase again. The lowest magnitude of failure stress attained in the graph for case 1 is at 30-60 degrees with the ratio of S to X decreasing up to 0.25. Failure stress behavior for case 2 and case 3 is similar but the decreasing rate in case 2 is slightly bigger than case 3. The curves for both situations have the same starting point and ending point as in all cases, but the difference in decreasing rate of failure stress is highest at 30 degrees. In case 4, the plot was different compared to case 2 and case 3. Failure stress was always decreasing with the increase in angle in case 2 and case 3, but in case 4, failure stress value grew at the angle between 0 to 30 degrees and started to decrease as in case 2 and 3, finally reaching the lowest at 90 degrees. Case 4 has three distinctly different values of slope for three sections of 0 to 30 degrees, 30 to 60 degrees, and 60 to 90 degrees. The slope was highest between the sections 30 and 60. As we already know that the ratio is always constant at 0 and 90 degrees for each data set under all circumstances, it is more important to see the ratio range in the angle between them i.e. 30 and 60 degrees. When the shear stress is 0.1*X, the ratio is almost constant for all the data sets at 30 degrees and 60 degrees. When the magnitude of ‘S’ is

lower, the ratio range calculated does not vary so much. As the magnitude of shear strength is increased the ratio range also increased to a higher number.

2.4.3 Malmeister Criteria

Table 4 Summary of Malmeister Criteria Result

S. No	S -Value	Average σ/X			
		Angle			
		0	30	60	90
1	0,1*X	1	0,35-0,36	0,30-0,33	0,35-0,57
2	0,3*X	1	0,93-0,96	0,46-0,69	0,35-0,57
3	0,5*X	1	0,98-1,07	0,47-0,72	0,35-0,57
4	1*X	1	0,98-1,11	0,47-0,74	0,35-0,57

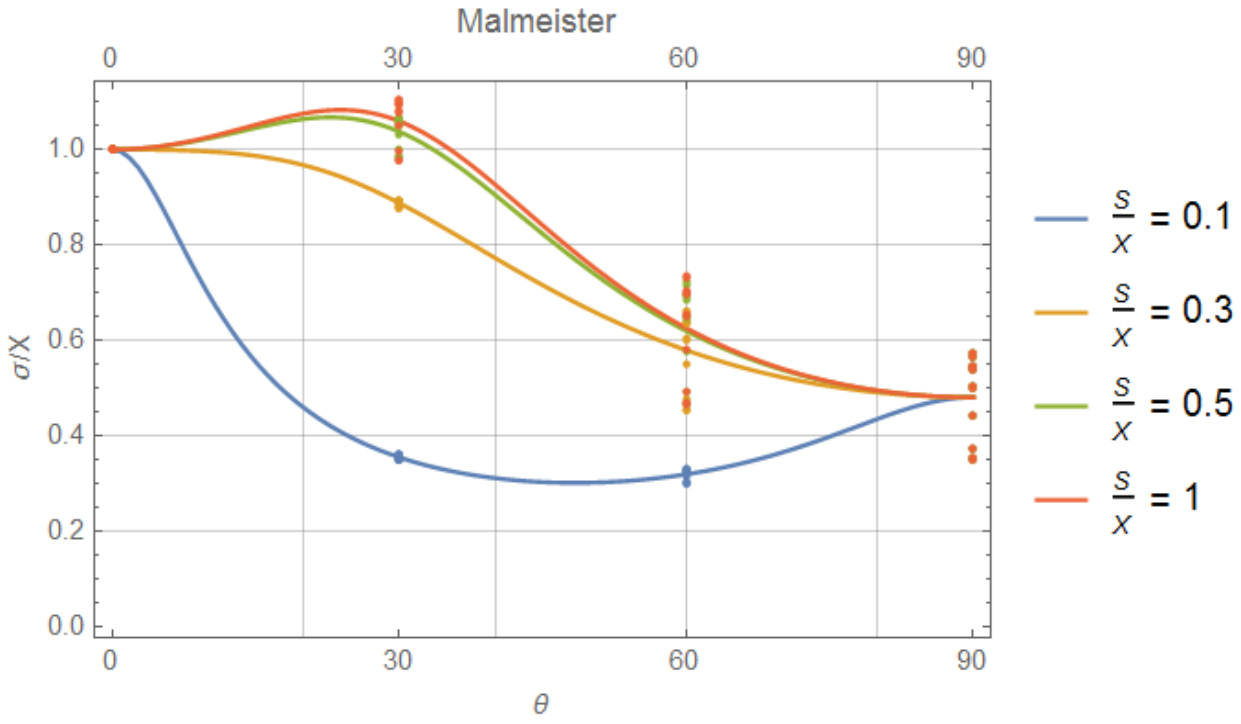

Graph 3 Graphical Presentation Malmeister Criteria Result

The result of the plot for the Malmeister criteria for the same input values and conditions as for previous two conditions can be found in above graph. For case 1, the characteristics of the graph are not so similar to previous conditions and the minimum magnitude of failure stress also increased from 0.25*X in previous two criteria to 0.35 * X in Malmeister criteria. Unlike Tsai-Hill and Max stress, the section between 30 and 60 degrees is not constant. Although the rate of change is small, failure stress is decreasing all the time, hitting the lowest at 60 degrees. Also, as the ratio of S to X increases,

the difference in the gap between two plot lines of different cases decreases. The difference in failure stress at the same angle but the different value of S decreases as the ratio of S to X tends to 1. The difference in the failure stress is very high when the value of S is increased from 0 to 0.4, but the difference when the S value is increased from 0.4 to 1 is negligible compared to the increment from 0 to 0.35 which created the big separation between graph lines when S = 0.1 and 0.35. From the graph, it can be deduced that beyond some point, the failure stress will no longer be dependent on S value or will have a very negligible effect. In cases 3 and 4, the value of failure stress between angle 0 to 30 increases slightly before starting to decrease. As in all previous criteria, the starting point of the plot and ending point of the plot is same.

2.4.4 Norris and McKinnon

Table 5 Summary of Norris and McKinnon Result

S. No	S -Value	Average σ/X			
		Angle			
		0	30	60	90
1	0,1*X	1	0,22-0,23	0,21-0,22	0,35-0,57
2	0,5*X	1	0,74-0,82	0,43-0,63	0,35-0,57
3	0,65*X	1	0,81-0,91	0,44-0,67	0,35-0,57
4	1*X	1	0,91-1,03	0,46-0,71	0,35-0,57

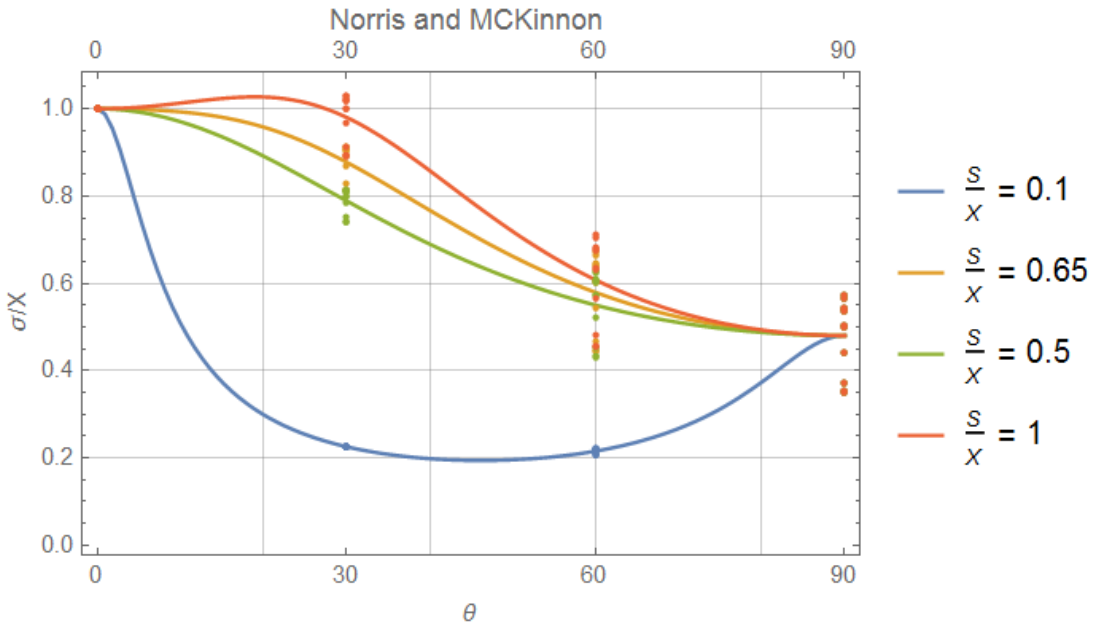

Graph 4Graphical Presentation Norris and McKinnon Result

Comparing, the above graph obtained for the Norris and McKinnon criteria with the graph obtained for the Tsai-Hill criteria, it can be clearly seen that the result are very close to each other. The characteristics feature for all cases are very much alike, but the magnitude of the failure stress is lower in the case of Norris and McKinnon. For example: in case 2, at 30 degrees and 60 degrees in Norris and McKinnon criteria, failure stresses are 0.7*X and 0.6*Y respectively. In Tsai-Hill criteria for a similar condition, failure stresses are 0.75*X and 0.65*Y respectively. Comparing these two examples shows that only the magnitudes are different but the characteristics of the graph is similar. If the value of S is taken slightly higher in the case of Norris and McKinnon compared to Tsai-Hill criteria, then it would produce the same result. When the value S tends to zero, then the failure stress value is same for all failure criteria explained above except Malmeister criteria. The graph line is same at S = 0.1*X compared to Tsai-Hill criteria.

2.4.5 Tsai-Wu Criteria

Table 6 Summary of Tsai-Wu Criteria Result

S. No	S -Value	Average σ/X			
		Angle			
		0	30	60	90
1	0,1*X	1	0,31-0,32	0,27-0,30	0,35-0,57
2	0,4*X	1	0,86-0,92	0,45-0,67	0,35-0,57
3	0,5*X	1	0,92-1,01	0,46-0,71	0,35-0,57
4	1*X	1	1,06-1,21	0,47-0,76	0,35-0,57

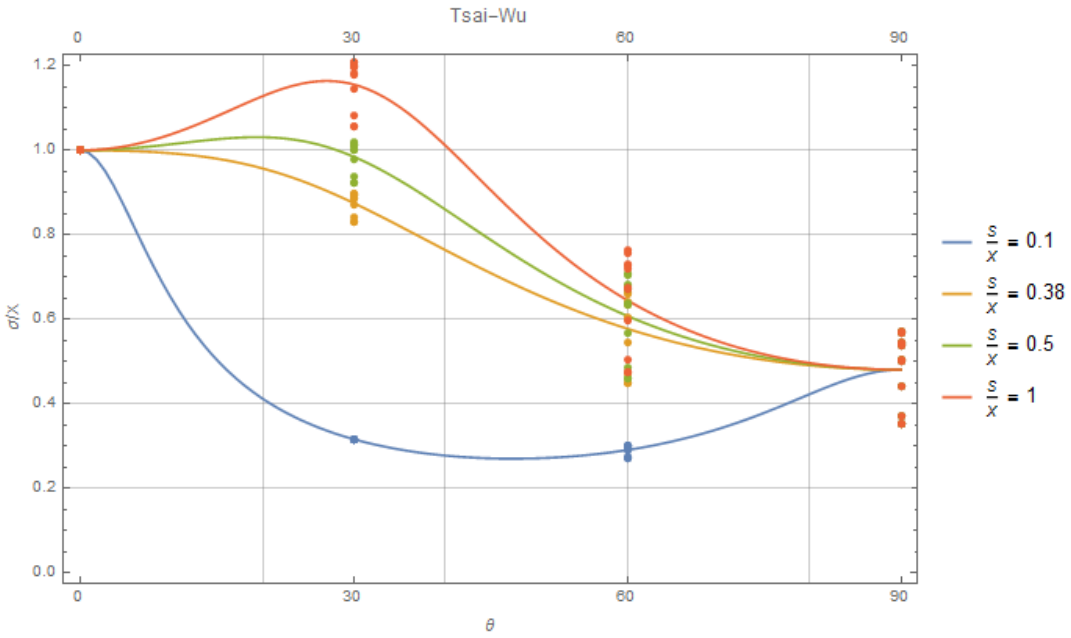

Graph 5 Graphical Presentation Tsai-Wu Criteria

As in all previous failure criteria cases, starting point and ending point for the graph is same. For case 1, the decrement rate of failure stress is very steep in the graph section 0 to 30 degrees, with a constant value between 30 to 60 and rising from 60 to 90 degrees. As the value of shear strength S rises, the slope of the first section of the graph i.e. 0 to 30 starts to decrease and is almost constant when the value is half of ultimate tensile strength. At the same time, the slope of section 2 and 3 of the graph i.e. 30 to 60 degrees and 60 to 90 degrees starts to increase with the increment in shear strength. Throughout the case 2 and 3, failure stress is decreasing all the time with the increasing magnitude of the angle. For case 4, failure stress first increased until the angle is increased to 30 degrees and it starts to decrease all the way to 90 degrees. The minimum value of failure stress is recorded 0.48 times the ultimate tensile stress when the layer orientation is 90 degrees for case 2,3 and 4, and for case 1 it is less than 0.3 at 60 degrees.

2.4.6 Lab Experiment Results

The data related to lab experiments are taken from the reference [25]. Uniaxial tensile testing was carried out to collect the data to observe the varying ultimate tensile failure strength with the increasing angle between building orientation and the applied load direction. Authors of both research papers, this and the research referenced [25], carried out research for the same institution and the same research area but with different perspectives. The following graph shows the result obtained from the experiments.

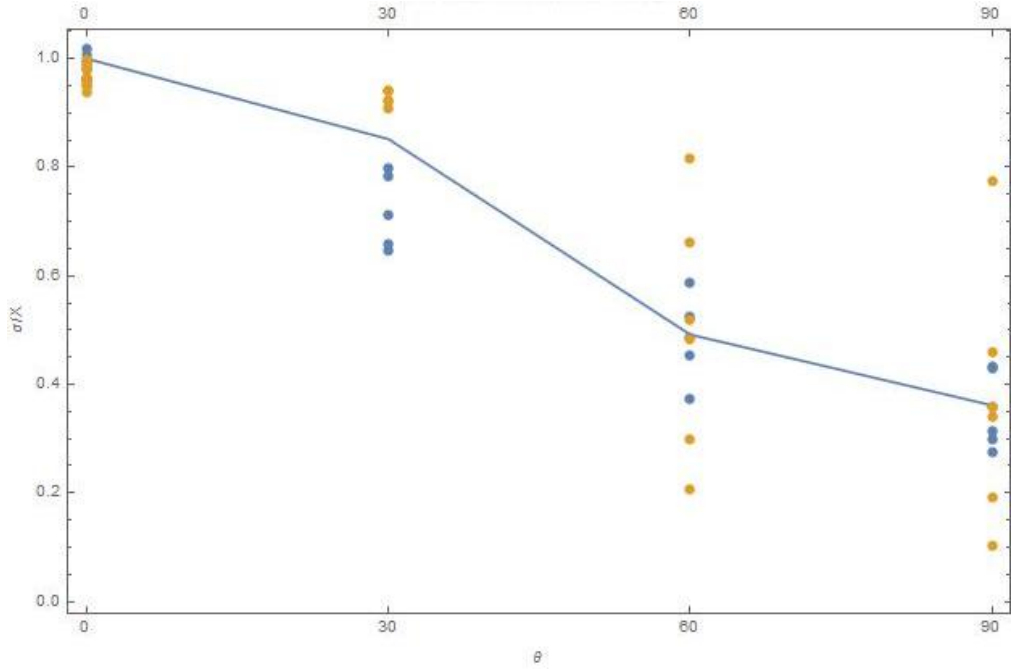

Graph 6 Lab Experiment Results

2.5 Theoretical Result comparison

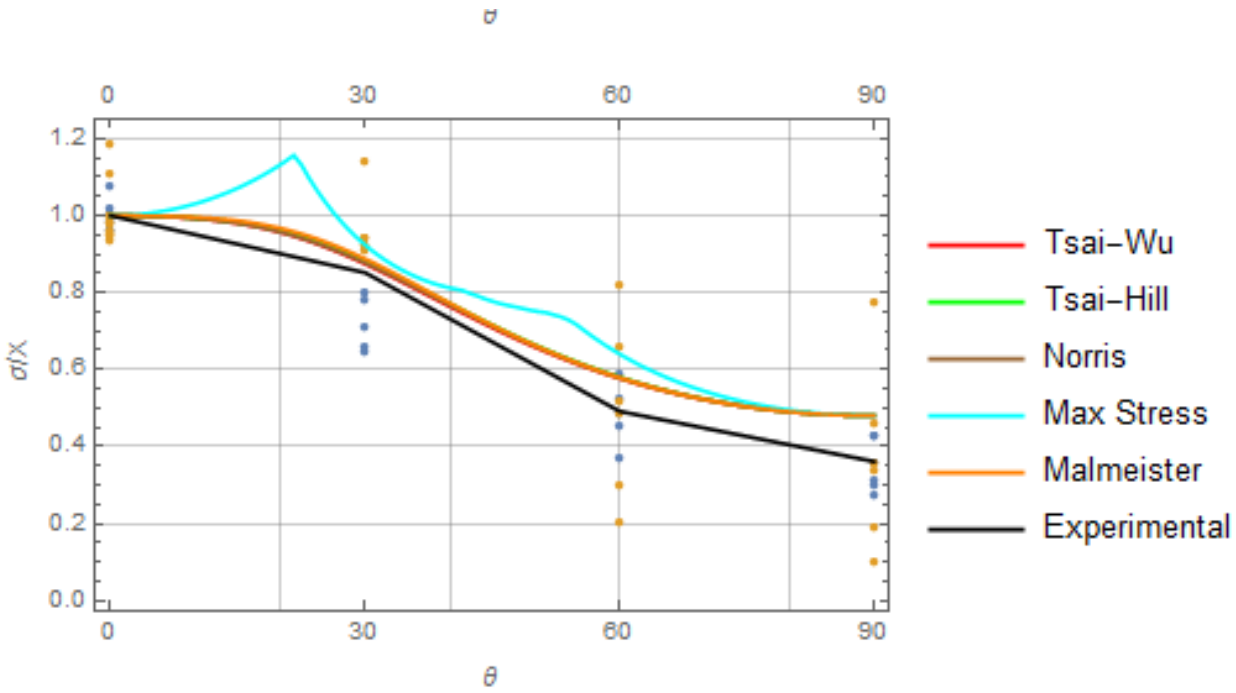

Graph 7 Result Comparison; All Results

All the results, obtained from calculation and analysis are collected in the same graph above. As seen in the sidebar, colors listed represent the theoretical result obtained from different failure criteria. When all the failure theories are compared to each other, except the maximum stress criteria all other theories are very close to each other. Accord-

ing to the maximum stress criteria, all three material properties i.e. X, Y, and S has an individual effect on the properties. Only one of those is dominant in the failure strength, and they do not have combined effect at any point with each other. In other failure theories those three material properties interact with each other and calculates the failure stress at each point which might be the reason of the difference in the result between the maximum stress criteria and other failure criteria. Results from all the failure criteria have the same starting point and ending point.

When these failure criteria are close to each other, the magnitude of shear strength 'S' is different in all failure theories. There might be other reasons behind this, and one of the most obvious reasons is these criteria are not developed considering the 3D printed materials but to composite materials. Contrast to the composite materials there is not only the layer orientation factor that affects the ultimate strength of the 3D printed materials. Few more parameters affect the strength properties of the 3D printed materials as discussed in the theoretical analysis section of this paper. For example bead width, air gap, contours, build temperature, etc. All these factors also affect the strength properties of 3D printed materials to some extent but the failure criteria for composite material do not take into account, the effect of those parameters.

Table 7 S-Magnitude comparison for all Criteria

S. No.	Failure Criteria	S-Magnitude
1	Maximum Stress	0.4 * X
2	Tsai-Hill Criteria	0.55 * X
3	Malmeister Criteria	0.3 * X
4	Norris and McKinnon	0.65 * X
5	Tsai-Wu	0.38* X

Above table includes the summary of the theoretical analysis of the failure theories, which shows the magnitude of 'S' taken to produce the result, close to each other. All the failure criteria show the different magnitude of 'S' from one another when the result tends to be as close as possible with each other. The maximum value of 'S' is found for Norris and McKinnon criteria with the value 0.65* X and the smallest magnitude of 'S' are for Malmeister criteria with the value 0.3*X. The smallest magnitude differs from the largest magnitude by more than 50% less. Other magnitude shown by other criteria's are 0.55*X for Tsai-Hill criteria and 0.4*X for Tsai-Wu criteria and Maximum stress criteria.

According to the data sheet produced by the manufacturer of the 3D printing materials, [18], [19], the ultimate shear stress magnitude is always more than 1.2 *X, but result shows the very low magnitude of ‘S.' The highest value calculated was 0.65*X which is lower than half of the value stated in the manufacturer’s data sheet.

2.6 Discussion

After studying the result and one on one comparison of the failure stress graph obtained from the failure criteria, it is easier to conclude the result. As seen from the result, most of the failure criteria have a different magnitude of ‘S’ from each other while the results being close to each other. The variation is so large that it cannot be neglected to draw any common conclusion or magnitude that fits all the failure criteria. The value of ‘S’ obtained from the data sheets of manufacturer does not match with values obtained for any of the failure criteria above. The highest value of ‘S’ is obtained for Norris and McKinnon and it is also almost half of the magnitude listed in the manufacturer’s data-sheets. When the resulting graph of all failure criteria is checked for the case S = 1*X, the failure strength value increases from 0 degrees until 30 degrees and slightly beyond, before it starts to decrease. The failure strength value never increases at any point according to previous research papers. These all findings show that the failure theories formulated for composite structures and other general materials do not work for 3D printed parts. A maximum stress criterion which is supposed to work for a very wide range of materials also seems not working in case of 3D printed parts

So, existing failure theories need some adjustment before using them for the strength prediction of the 3D printed parts, or an entirely new theory should be researched. It is not hard to conclude that the lamina failure theories cannot be used directly for the purpose of strength modeling of 3D printed parts based on the above findings.

2.7 Further Proceedings

After careful consideration of the result obtained from the literature review and analysis, it is very hard to conclude that the 3D printed parts behave in a similar way as in composite materials. Using lamina failure theories to predict their strength without any amendments or further research seems unwise after considering the results of the analysis done in this research. Most of the researches carried out in the area of failure prediction of 3D printed products are based on the comparison with each other with different layer orientation. Few research papers have also predicted the failure by comparing the

strength with the similar parts manufactured using other techniques for example molding. Displacement and strains are very important factors in failure process. Most of the research have overlooked these particular terms while researching the failure in the 3D printed products. Thus, taking into account of the research done until this point for this paper, it is noteworthy idea to take a step back and try to research and find the influence of displacement, deformations, strains, crack initiation and propagation first to move forward with strength modeling of 3D printed parts.

If we look closely at the end product fabricated by two different technique, 3D printing, and molding, they are totally different. Even though the same product with same dimension, shape, and size are produced, they exhibit properties in a different way. The material in the molded end product is isotropically distributed, and the whole end product behaves as a single unit so, material failure theories effectively work in those products. Corners and edges are mostly smooth in molded end products. It is very difficult to tell where the initial crack starts to develop in such product but the use of material failure theories can closely estimate the failure stress. The end product from 3D printed parts has some difference in regards to the material distribution. It is built by adding a layer on top of previously added layer, and that makes the end product as the several bonded layers. If we just take two layers and analyze it, then each layer might be equally strong, but the bond between them might not be equally strong. Corners and edges in 3D printed parts are very rough if the end product is examined properly. So, 3D printed parts are vulnerable to fail not entirely due to material failure but also from the built up defects that occurred during manufacturing. All these facts define 3D printed products more as a structure. So, it seems beneficial to research on the failure mechanism of 3D printed parts as a structural failure as the failure depends on more parameters rather than just material failure. It is easier to imagine the failure modes if the end product from molding is compared to the brick and the 3D printed parts are compared to the walls that are made from hundreds of such bricks. The failure in bricks and walls can frequently be seen which do not require any proof that the failure in those two is different from each other.

Considering all these facts, theoretical analysis and studies from previous research papers, strength and failure prediction of the 3D printed parts is not developing towards a satisfying result. On the other hand, the popularity of 3D printed products is increasing more and more. Previous research papers have been able to answer few questions but not completely as most of the researches are done only in material level and not to

the structural level. It is wise to take a step back and analyze the failure, occurring in the mechanically loaded 3D printed parts under different circumstances i.e. displacement, deformation, strains, crack initiation, to continue with the research in this field. Digital Image Correlation (DIC) is the handiest tool to study those details.

2.8 Digital Image Correlation (DIC)

DIC is a method of tracking and comparing images of the object under some actions (under loading conditions generally in mechanics) to measure the changes in those images. Changes are easier to observe as the method use small blocks of pixels called as subsets from the image taken and compare the positioning of the same block of pixels in the next image with other neighboring blocks of pixels. This technique uses digital charged coupled device (CCD) camera to take the image of the surface of the object under observation. Under the camera, the surface of the object should be illuminated in the wide range of contrast and intensity levels so that it is easier to distinguish the blocks of pixels. It is done usually by either painting speckles on the surface or mostly the texture on the surface of the test specimen is itself sufficient to create enough contrast and intensity levels to produce analyzable images. The method is capable of measuring the changes in micro and nanoscale. Changes are seenand can be measured in 2D and 3D with the use of multiple cameras. The method is proven accurate enough by comparing it to valid FEA models which make the method feasible for many applications. [28, 30] Hence, the most important part in DIC is image matching.

Images used in DIC are generally of high resolution as it is used to research the engineering aspects which require analyzing the changes in the micro and nano level. According to Sutton [34], to accurately reduce the strain-stress curve from the images, change in the displacement of order 10^{-5}m/m is best to consider. So, there is no wonder that the camera used for DIC purposes produces high-quality images to meet the threshold. There are few things to keep in mind before image matching, aperture problem, correspondence problem and speckle patterns. One particular image pixel is not possible to compare with another image pixel as the multiple similar pixels might be present in another image. Hence, making correspondence considering only one pixel is not possible. Instead, the speckle pattern present in a small neighborhood called as a subset is compared in two images to make the proper correspondence. Such subset is created either by the texture of the surface of the specimen itself or by painting or spraying. It enables a more accurate way of tracking the motion of material flow when deformation

happens. Following are some of the applications, where DIC can be used in mechanics of materials.

- Material testing (defining material properties for example young's modulus, Poisson's ratio, etc.)
- Fracture Mechanics (crack initiation and growth)
- Dynamics Measurement (example vibration)

2.8.1 DIC Software

There are different ways of matching the images and mathematically formulating it to calculate the deformations and strains. Measuring displacement and strain using DIC has been in use for a while now. These days fully automated DIC software based on a different algorithm developed by researchers are available that calculates the deformation, strains, dynamics, geological mapping, etc. processing the image obtained from the tests. Software deploys different algorithm to quantify the test results. Different algorithms have already been developed for image matching in DIC. The application field of the DIC is so broad that researchers from different fields have developed different algorithm specializing in their respective area of research. Algorithm for such software is the mathematical formulation to quantify the result obtained from images taken during the experiment. For instance Sutton [34] explained the differential method and template matching method to determine the 2D displacement of the subset and used shape functions to predict the deformation of the subsets. Later on, the differential method is developed to predict the 3D displacement too. [31]

Due to the development of such DIC software, measuring deformation, displacement, strain and tracking crack initiation and growth has become fairly easy and accurate to determine the material properties. Displacement and strain are very important parameters in determining the mechanical properties of the materials. DIC is well suited for measuring them as it measures the difference in the object from smaller loads to bigger loads. The author of the article [28] claims that it is even possible to see the difference in the bridge because of a bird landing on it, using the DIC. Cracks which are the major reasons of failure in both structures and materials is seen with DIC that are not readily visible to the naked eyes [31, 32, and 33]. DIC is in use to study deformation behavior in different types of material since the 1980s and has been able to produce the significant results for metals, plastics, woods, composites concretes, and other materials. DIC

is in use to research deformation for both materials and structures, and most of the research uses the technique of matching subsets to determine the displacement [34].

Crack initiation and propagation in 3D printed parts under the effect of loads is important factors to research. 3D printing is not one of the clean manufacturing processes as the final product has inbuilt defects. It is obvious that 3D printed products usually do not have a smooth surface that results in many high-stress concentration points in the product that increases the chances of premature failure of the material. DIC is well equipped to track the crack formations that are not visible to naked eyes too and also the crack propagation studies will open new insights about the failure in 3D printed parts. Since 3D printed parts are made of layers on top of previous layers, it would be interesting to see the crack propagation between those layers. [29]

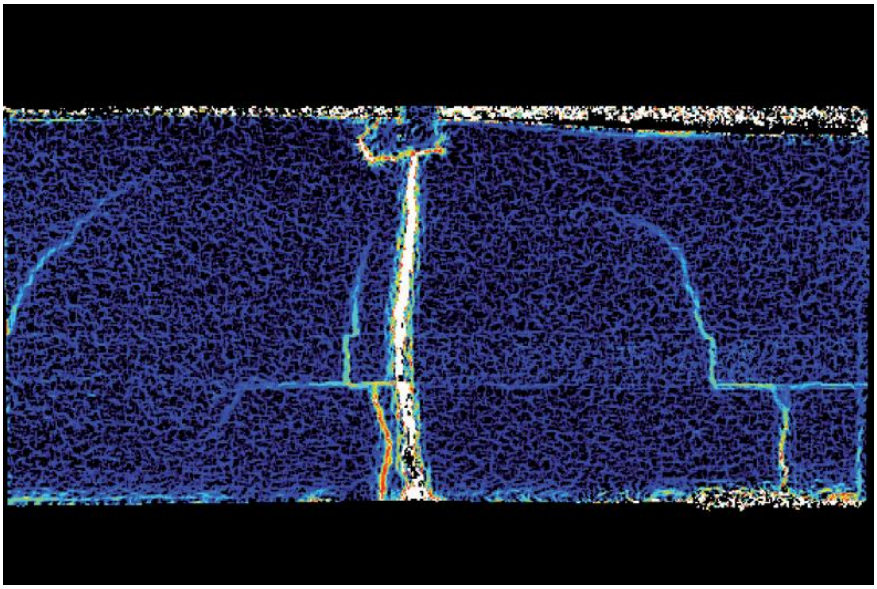

Figure 7 Cracks not visible to naked eyes but visible to camera [28]

The algorithm used to analyze the test result in this research project uses the Least Square Image Matching (LSM).

2.8.2 Least Square Image Matching (LSM)

Image matching has broad applications and some working principles that work behind image matching. The key objective of image matching is to figure out the matching pixel in the same physical region. Key point matching, area-based matching, intensity based matching, are few mostly used matching methods. [35] LSM method gives a mathematical description which falls under an area-based matching so, it is highly accepted for the research purposes. Compared to other methods, LSM has higher accuracy in image matching. The results obtained from LSM have the accuracy of 1/10 pixel or even better. However, being a non-linear process, close approximate values are re-

quired in this method. According to the author of the reference [36] LSM has the dual advantage of area-based matching process and edge based matching process if it is used to its full potential. Some other potentials of the LSM method as exactly described by the author of reference [36] are listed below in his words.

- High matching accuracy
- Geometrical/stochastical constraints: stabilization, reliability, speed
- Multi-image matching (reliability)
- Simultaneous matching/point positioning
- Multi-patch matching: neighborhood conditions
- Multispectral, multi-temporal matching
- Monitoring of quality (precision, reliability)
- Simultaneous image reshaping, radiometric adjustment
- Combination of area-based and edge based analysis
- Usable in hierarchical mode(coarse to fine)
- Usable as derivative operator based matching procedure (first order, slope variable, second order)
- Rule-based matching: patch selection (good signal content)
- Incomplete data patches (for example, triggered by conclusions)
- Computational performance: parallel implementation possible
- Usable for pattern recognition (template matching), feature extraction, image feature measurement, change detection, line following
- General matching technique (beyond images)

LSM is in use for almost three decades now and has constantly been modified to yield better results, accuracy and to address the specialty of the problem properly. The general mathematical formulation of the LSM is stated below.

$$g_1(x_1, y_1) = h_0 + h_1 g_2(a_0 + a_1 x_1 + a_2 y_1, b_0 + b_1 x_1 + b_2 y_1)$$

Where,

g_1, g_2 is intensity of reference image and the querying image respectively that depends on upon image coordinate x and y

a_i and b_i are the unknowns in the affine transformation model

h_0, h_1 are the unknowns in the linear model of intensity

As shown in the equation above, the general principle behind LSM is to define the relation between two different patches of the same size in different images. Then affine

transformation model is used to show then intensity variation using geometry and linear model description. Now, Using Taylor linearization, transforming above function into linear function we get-$g_1(x_1, y_1) - h_0 - h_1 g_2(x_2, y_2)$

$$= dh_0 + g_2(x_2, y_2)dh_1 + h_1\left(\frac{\partial g_2}{\partial x_2}\right)da_0 + h_1 x_1\left(\frac{\partial g_2}{\partial x_2}\right)da_1 + h_1 y_1\left(\frac{\partial g_2}{\partial x_2}\right)da_2$$

$$+ h_1\left(\frac{\partial g_2}{\partial y_2}\right)db_0 + h_1 x_1\left(\frac{\partial g_2}{\partial y_2}\right)db_1 + h_1 y_1\left(\frac{\partial g_2}{\partial y_2}\right)db_2$$

3 Experimental Setup and Procedures

Experimental setup for the testing is relatively easier and inexpensive than most of the other material testing setups. The main task of the experimental setup is to direct and fix CCD camera towards the experimenting test specimen and connect it with correlation software through a computer or other possible instruments. As the test proceeds, the camera captures the image of the whole process and sends the image for further processing to correlation software. [30] However, there are some important points to be considered before actual testing starts. When software and camera are ready, it provides live feed making easier to adjust testing conditions. Following are the few important parameters to adjust before testing starts.

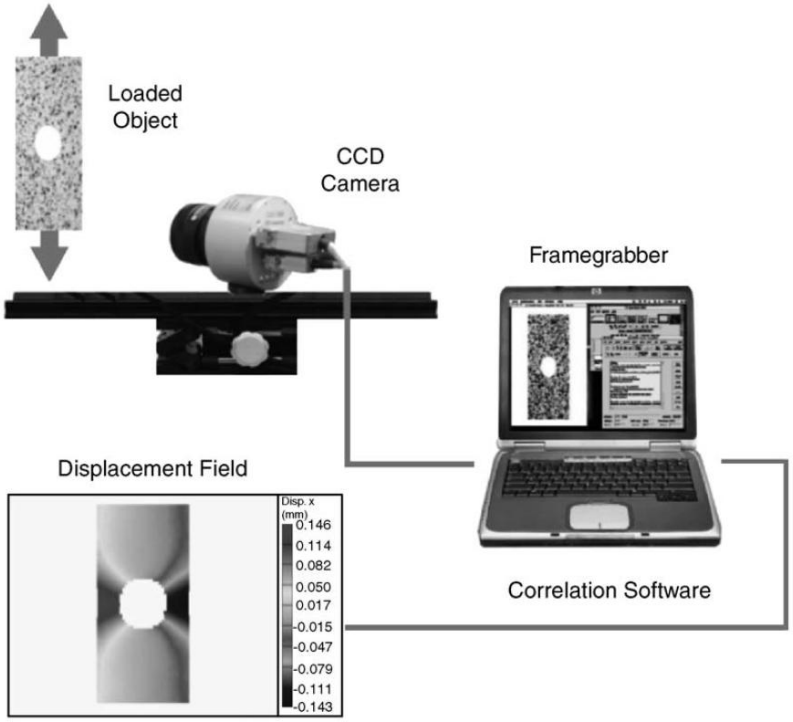

Figure 8 DIC Setup [30]

3.1 Lighting Conditions and Camera Focusing

After the testing is carried out, all the results are obtained from the study of images. Hence the lighting adjustments are one of the important parameters to consider carefully. Additional lights are used depending on the experimental environment. Neither, too bright light nor too less light can be afforded on the test specimen surface. Strong intensity of light on the test specimens causes the light reflection from the test specimen surface showing shiny part of the sample in the image and hiding the information under that shiny part. Less intensity of light on the specimen causes the dark patches and shadows of the surroundings and makes it difficult to see the details in the images clearly. The aperture of the camera is important in fine tuning the lighting conditions after the proper amount of light is cast on the test specimens. Indirect lights that are reflected and focused on the test specimens from other shining backgrounds (which are not in the focus of camera) can be a good option to get the ideal lighting conditions.

When measuring the 3D full field displacement, multiple cameras are used. Similar, to the ways that human eyes get a perception of 3D view, multiple cameras can generate enough information in 3D measurement. Both cameras should be focused to capture the area of interest. Only the common areas that are visible on both cameras can be analyzed in 3D. It is common that each camera has its unique area that is not visible in another camera; such area is not used while processing the result. It is important that the area of interest must be visible on both cameras. The angle of projection between two cameras should be appropriate which neither can be too wide nor too narrow. The wide projection has the big area to focus which may result in unclear information from the area of interest whereas narrow-angle projection gives less information on 3D measurement.

3.2 Calibration

Image calibration is an important part of the experimental setup and carried out after the area of the interest in the specimen is already focused. Calibration defines the position and orientation of the camera and the test specimen in the space in the coordinate form. After confirming everything are in place and will not be moving anymore especially camera and its focal length, calibration is done to set up the reference to determine the real size of the test specimen and deformation occurring in the test specimen. Calibration gives the information about the distance of the camera from the images in the coordinate forms to the software being used to quantify the size of the specimens and

deformations accurately. Calibration is done using the appropriate type of the calibration panel which helps to calculate focal point, principal points, distortion parameters, and translation vector and rotation matrix.

3.3 Specimen Preparation

DIC depends on the surface texture of the specimens recognized by the software as contrasting field whether it is naturally occurred, projected, painted or sprayed. There is not much; one can do if the test is carried out with naturally occurred patterns. However, most of the test specimens require painting or spraying to create the speckle pattern. Artificial ways of creating speckle patterns is always an alternative to create the good patterns The good pattern yields better results than naturally occurred contrast fields. Hence, it is important to consider few parameters to create the best possible patterns. Patterns should not be repetitive and isotropic which creates confusion in tracking the right one. Patterns made should be as high contrast as possible. DIC tracks the small groups of pixels called subset, and the patterns should be big enough to be seen and recognized and small enough at the same time so that the whole patch does not contain only one pattern. Normally, 2 to 5-pixel size is considered to be the good size for patterns. [37]

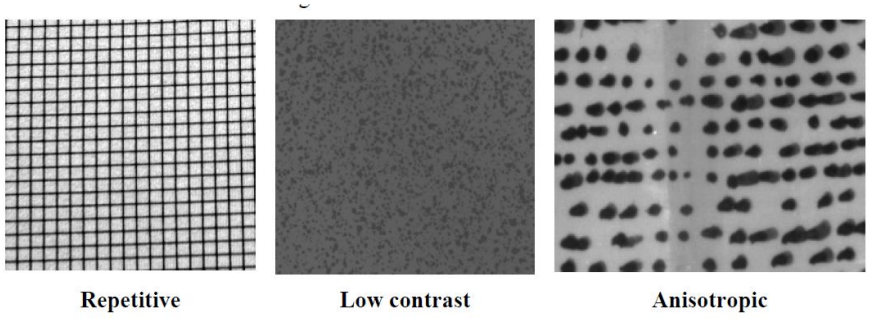

Figure 9 Invalid Patterns

Few ways to create patterns are discussed below:

- Spraying/Painting: The most common method for creating speckle pattern. It uses paint or spray paints on the specimen surface
- Toner: Toner powder is used to create the patterns. It can be done by dropping the specimen on the powder and gently blowing the powder until acceptable patterns remain.
- Lithography: Lithography or vapor deposition is used to create the patterns.
- Stencils: Stencils are rolled on the surface of the specimen. Patterns created are somehow uniform but contrasting and diverse enough to support the test.

- Printing: Printing pattern on paper and then gluing it on the surface of the specimen.
- Ink: Ink is dotted on the surface of the specimen to create patterns.
- Projecting: Especially, it is used for shape measurement. Patterns are projected using the projector. It should be optimized using the lighting conditions.

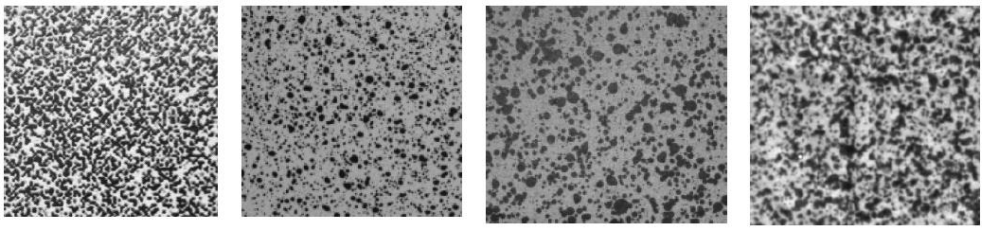

Figure 10 Example of good patterns

4 Test Specimens

In isotropic material, standard shaped test specimens are normally used to define the material properties. These test specimens are defined according to some test standards for example ASTM or ISO after years of research. They are well suited to answer most of the questions in material testing. 3D printed products are different compared to those materials. Although the printing is done using the isotropic material, the way of manufacturing makes the final product anisotropic. Using the same techniques and similar test specimens for experiments will not answer all the questions as in other isotropic materials. Many researches are done considering the similar techniques and similar test specimens, but the findings are always confined at one point. They are productive to address few questions but not good enough to kill all queries. For instance, research works that have been carried until now have found the ways to build the strongest 3D printed products but still not any research has been able to answer how to calculate its strength. Almost all the research works done in this field has been started from adopting some standard shaped test specimens and trying to analyze the result. So, the findings are always confined at a point. The used test specimens were not designed for testing 3D printed products so, the prevalent approach of researching in this particular area needs to be corrected somehow.

3D printed products were collected that can be mechanically loaded which are used as test specimens. Collected 3D printed products vary from one another. The ways, they are loaded mechanically are different from each other. Some of the test specimens are loaded under the bending moment, some with torque, tensile stress, and compressive

stress. The failures under all those circumstances are compared and analyzed to carry the research forward. DIC is well suited to cover all those variations in testing. DIC can be used efficiently to analyze the phenomenon going while testing those test specimens. All the test specimens collected are printed using the uPrint SE 3D printer manufactured by the Stratasys. According to the manufacturer, the machine builds the objects with the layer thickness of 0.254 mm. All the test specimens were printed using the material ABS plus thermoplastic as printer can print only ABS plus thermoplastic as building material. ABS plus has ultimate tensile stress (X) of 31 Mpa and ultimate shear stress(S) of 35 Mpa. More technical specifications for both printers and materials are available in the manufacturer's database referenced as [18] in this article.

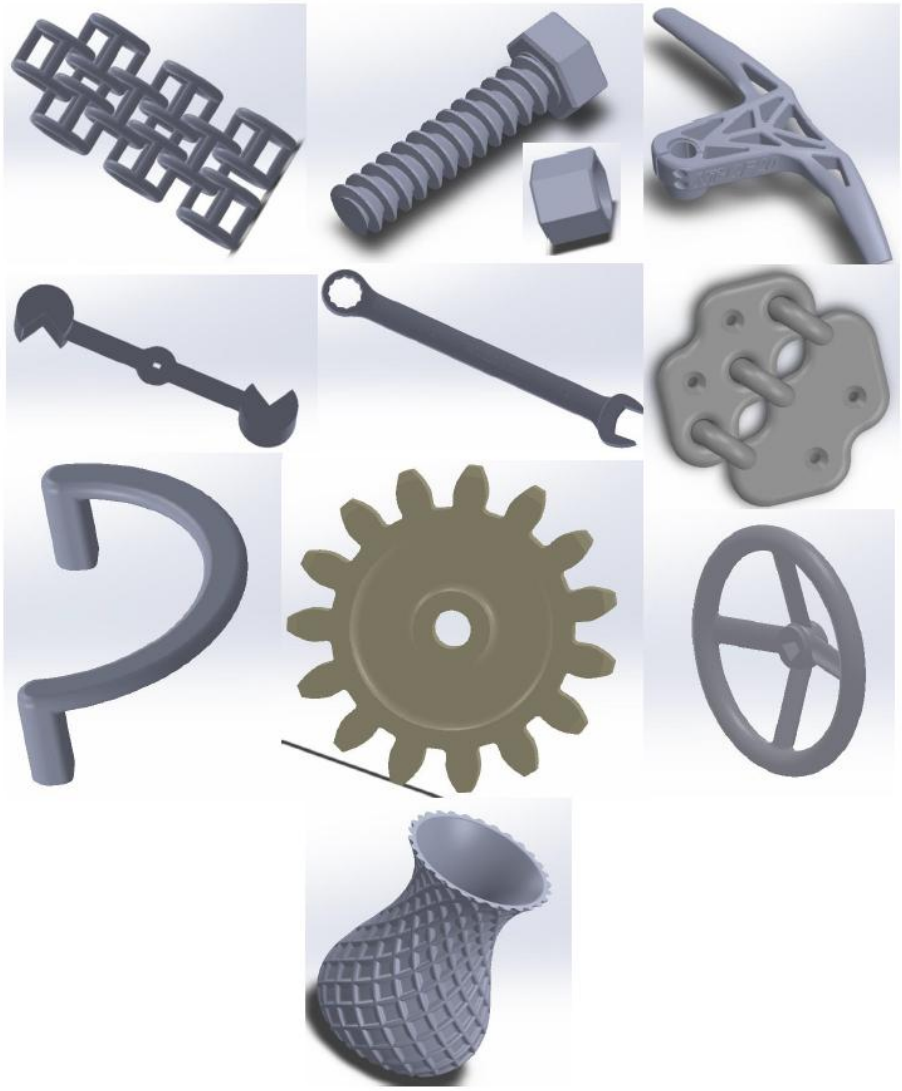

Figure 11 Test Specimens

5 Experimental Results

The images captured from the DIC set up were analyzed using Davis LaVision software. The number of the images from each test depends on the amount of time; they resisted the applied load before failure. For all tests, image capturing rate was 100 frames per second. So, each test has minimum thousands or even tens of thousands of pictures in some cases. It is neither easy nor is important to analyze all the pictures to calculate the strain field. The reason behind taking such large number of pictures is to make sure that the important moments during the experimentation is not missed. So, from each test, appropriate numbers of images after constant intervals were classified from the bulk to analyze.

Primarily, the strains on the test specimen at the failure area were calculated if the failure area is visible in the camera focus. Strains are then compared with the force obtained from the testing machine. Some of the specimens failed at the points that were not visible in the camera or out of focus. The areas where the cameras were focused on such specimens were used to extract the strain behavior of the sample on those areas. Graphs depict the strain relative to the preceding image starting from the strain zero conditions. All three strains (E_{xx}, E_{xy}, and E_{yy}) are extracted and studied from the Lavision software.

High-resolution images were taken separately from the fracture surfaces of the test specimens after the experiment. The important factors behind the failure that are not obvious to the naked eyes are visible from the high-resolution camera images. The causes and nature of the failure surface of each test specimens and the force associated with the failure are discussed that are visible in the images.

Test results are categorized under different test specimen heads, and each head has two sub types namely fracture surface analysis and DIC results.

5.1 Test Specimen 1 (Gear)

The strength of the 3D printed gear teeth was tested with the DIC setup as explained in the experimental setup. The same gear was experimented three times with different teeth as the building orientation of the teeth was different from each other. Following figure shows the test setup for the gear setup.

Figure 12 Gear Experimenting Setup

Gear was fixed from the top, and the structure that is hooked to the teeth was pulling it down. The rate of pulling down in terms of displacement was 1mm/min. The force that caused the failure of the tooth was mostly shear force. Depending on the teeth building orientation the result of the failure was different and explained in detail below.

5.1.1 Fracture Surface Analysis

- 0-degree orientation

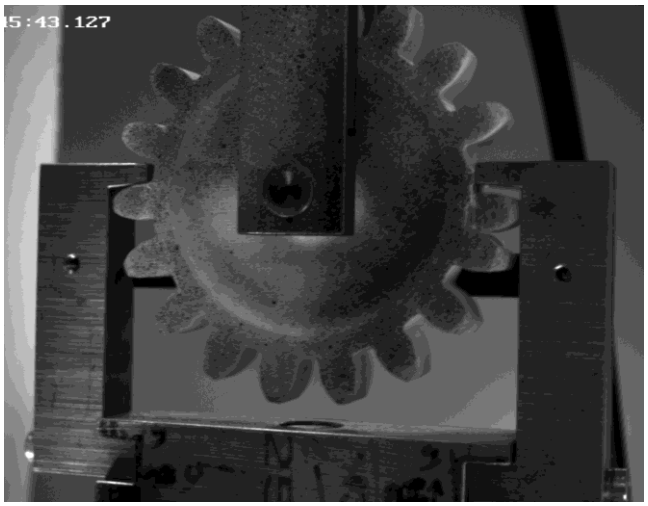

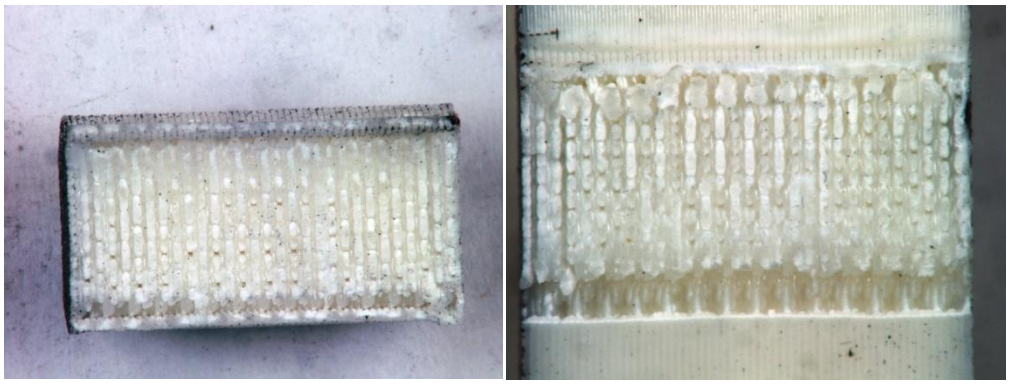

Figure 13 Failure in gear tooth (0 degrees)

The building orientation of the tooth is parallel to the force in action. The failing teeth totally snapped from its place and got separated from the parent piece. The failure was similar to the brittle materials like ceramics and glasses that shatter when the enough load is applied. Failure surface was in the same plane with each alternating layer. The odd number layers were broken at one plane, and even number layers were broken at another plane and the difference between the broken planes is very negligible that the failure surface can be counted as one plane.

- 45-degree orientation

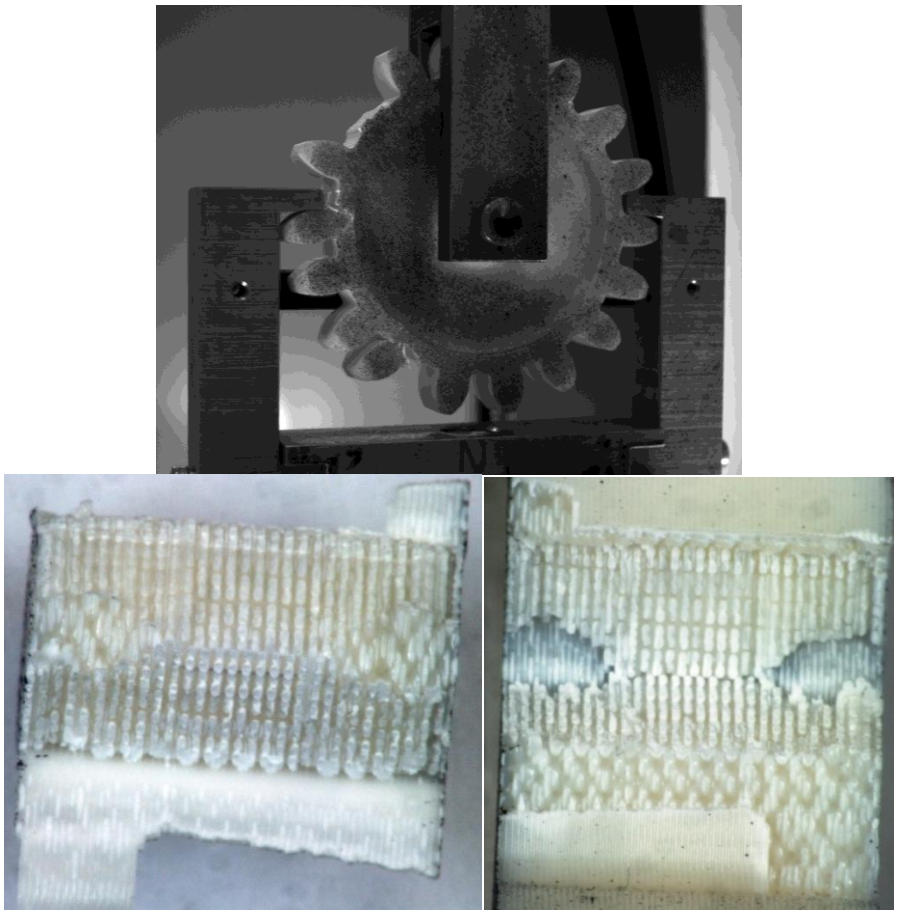

Figure 14 Failure in gear tooth (45 degrees)

The failing tooth did not completely separate from the parent piece and had a different way of failure compared to the tooth with 0-degree building orientation. The crack started to originate from the edge of the tooth and gradually increased towards the center of the parent material. After some depth is acquired the direction of the crack propagation changed towards the lower edge of the tooth. The experiment was aborted before the tooth was totally separated. The tooth was later separated from the parent piece to study the failure surface. As seen in the pictures of the failure surface, the direction of the crack propagation was changed when the depth of the crack reached the half of the height of the tooth. The noticeable thing at the point where the propagation direction was changed was the different pattern of the failure compared to rest of the failure surface.

- 90-degree orientation

  The force in action was perpendicular to the building orientation of the tooth and generated failure shown in the picture below.

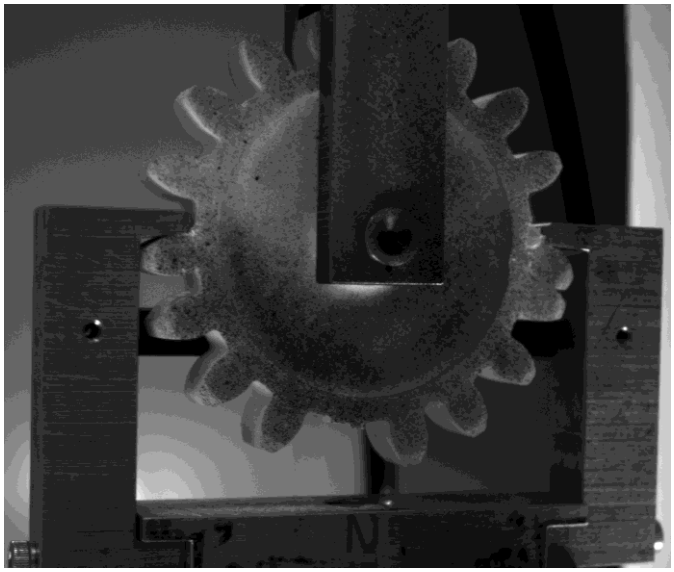

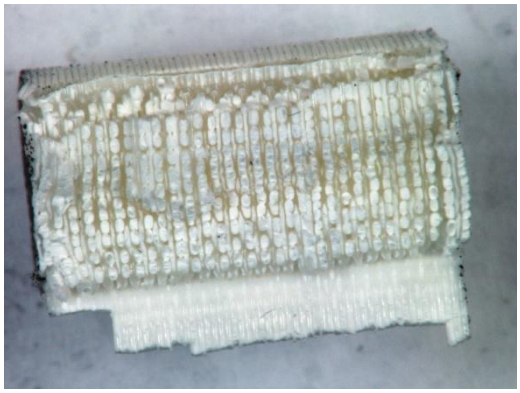

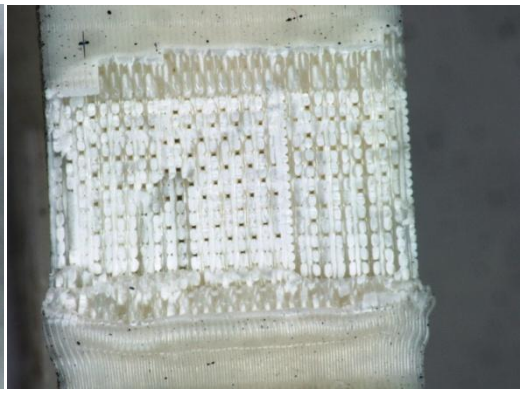

Figure 15 Failure in gear tooth (90 degrees)

Crack propagation was not on the same plane, and it was not predictable either. The failure surface was not as clean as in previous two cases. Some of the layers were delaminated from both parent piece and the failing tooth. It caused the non-uniformity in the fracture plane and the bending of the layer in broken piece. Before the failing piece separated from the parent piece, the tooth hit the adjacent tooth. The tooth was separated later to study the failure surface.

5.1.2 DIC Result

The amount of time the gear resisted the load was different to each other according to the angle between the line of action of the force and the layer orientation.

- 0 Degree orientation

Table 8 Test Summary (Gear 0 degrees)

Number of images captured	About 14,500
Test Duration	About 150 seconds
Failure occurred at image number	13,848
Number of images taken for strain extraction	30 (After each 500 starting from zero until failure image)
Force associated in failure	Shear force parallel to layer orientation
Maximum strain in X-axis E_{xx}	0.15
Maximum shear strain E_{xy}	0.96
Maximum strain in Y-axis Ey_{y}	0.04
Maximum force	4.3 (KN)

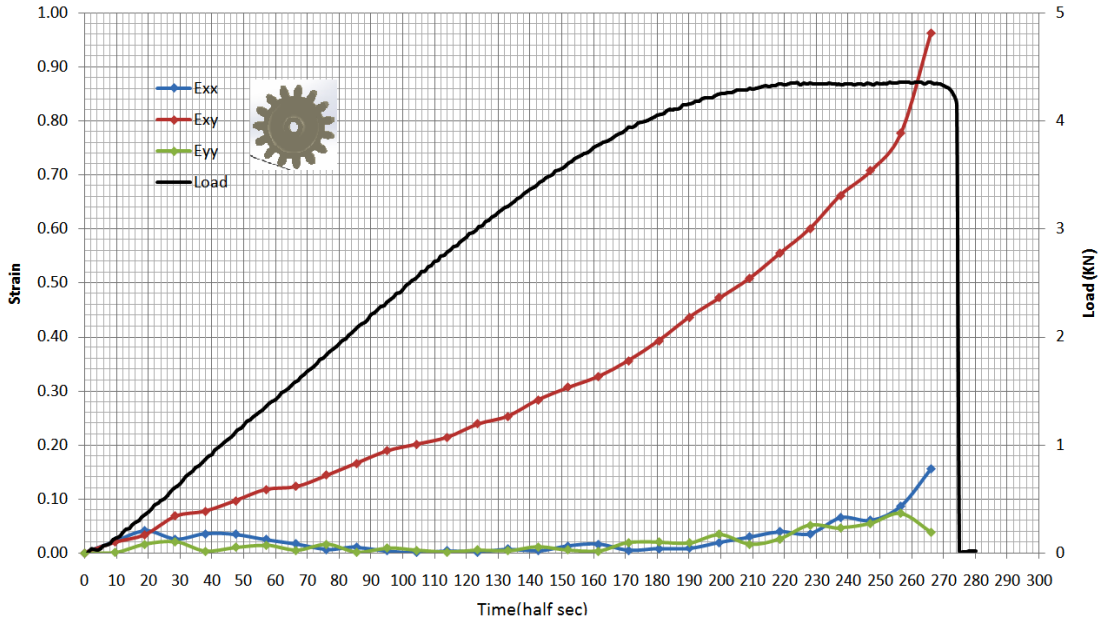

Graph 8 Loading and Strain Curve (Gear 0 degrees)

Most of the damage seems to be done by the shear strain. Shear force was the major force that was acting at the tooth. Applied shear force was parallel to the building orientation. The rate of development of shear strain was proportional to the increasing force. Strain in x-direction and y-direction are negligible compared to shear strain. Although shear strain was effective, the magnitude is less than 1 percentage. There was not much displacement before the failure. The failure happened very much to the like of brittle materials with no neck formation, and the fracture happened without much crack appearance. Loading curve is increasing smoothly without showing any sign of force release phenomena like a crack initiation or specimen slipping out of its place.

❖ 45 Degree orientation

Table 9 Test Summary (Gear 45 degrees)

Number of images captured	About 14,000
Test Duration	About 150 seconds
Failure occurred at image number	14,010
Number of images taken for strain extraction	30(After each 500 starting from zero until failure image)
Force associated in failure	Shear force at about 45 degrees with orientation
Maximum strain in X-axis E_{xx}	1.4
Maximum shear strain E_{xy}	0.72
Maximum strain in Y-axis E_{yy}	0.68
Maximum force	4.5 (KN)

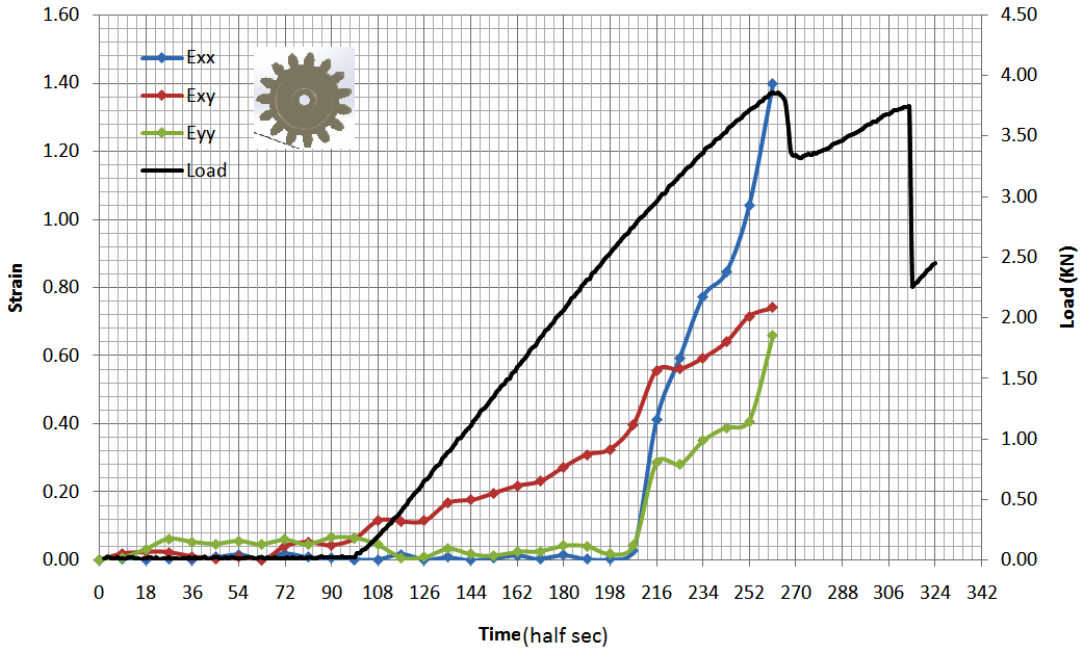

Graph 9 Loading and Strain curve (Gear 45 degrees)

Load stayed at 0 magnitudes for some time due to the gap between the specimen and the force exerting part. At those moments, all the strain parameters also stayed at almost 0 values, despite negligible noise due to specimen movement caused by a loose fitting. Both load and shear strain curve started to rise from the same point. This trend contin-

ued until the failure. At about 198 seconds all three strain parameters had a steep slope. Crack initiation might have caused it. Strain in x-direction and y-direction grew rapidly whereas shear strain constantly grew when the crack started to grow. Due to the crack opening, displacement in x and y-direction was more compared to shear deformation. Before the crack initiation, strain in both x and y-direction was silent. Hence, the shear strain was more responsible for crack initiation and failure. As seen from fracture surface, crack propagation has changed its direction at some point which is the good reason behind the steep fall in loading curve at around 260 seconds. However, displacement after the change in the direction of crack propagation was not calculated due to large deformation which requires different setting in the software used to calculate the strain. It was not worth to spend time behind that as the major damage was already done to the specimen.

- 90 Degree orientation

Table 10 Test Summary (Gear 90 degrees)

Number of images captured	About 35,700
Test Duration	About 350 seconds
Failure occurred at image number	35,632
Number of images taken for strain extraction	30 (After each 1000 starting from zero until failure image)
Force associated in failure	Shear force perpendicular with layer orientation
Maximum strain in X-axis E_{xx}	1.1
Maximum shear strain E_{xy}	1.5
Maximum strain in Y-axis E_{yy}	0.3
Maximum force	3.8 KN

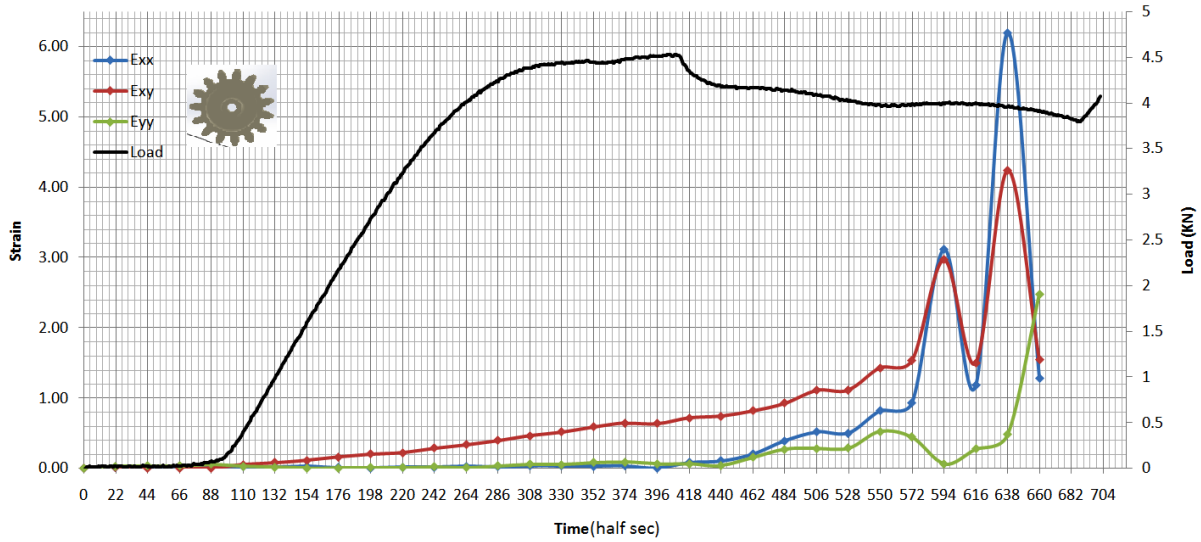

Graph 10 Loading and Strain Curve (Gear 90 degrees)

Similar to previous gear case, load started to increase sometime after the test started and has the same effect. Once again shear strain played the major role in failure as in previous two cases. The reason behind this is very clear. In all three cases, pure shear force is applied as the load. Shear strain is slightly higher in this case, than the previous case. It is almost double than the previous two cases. Around point 415, loading curve has fallen slightly indicating the crack started to propagate. From the very point, strains in x and y-direction started to rise. Until the crack initiated, shear strain was the sole reason for the failure. Since the specimen did not break into two separate pieces, it continued to resist the load. However, resistance was lower than crack opened. Between 682 and 704, load started to rise again after a long period of decreasing load. The failing tooth touched the adjacent tooth which increased the load resistance. Fluctuation in the strain values towards the end is due to the irrational behavior caused by the big crack opening.

5.2 Test Specimen 2 (Bike Handle)

The smaller scaled version of the 3D printed bike handle was tested with the previously mentioned DIC experimenting setup. Specimen was fixed at the same point as it meant to be fixed in real life situation. Load was applied on two ends of the handle. The direction of the load was downward pushing the handle at the rate of 2mm/min. When the load applied was enough to break the handle, it broke from the point where it was fixed. The force that caused the breaking was a normal force and the line of action of the force was perpendicular to the raster orientation.

5.2.1 Fracture Surface Analysis

The fracture surface was out of the camera focus, and it barred the view to study the crack initiation and propagation. However, the breaking was very close to that of brittle materials. Failure surface is then studied later on with a higher focus on the failure surface with the high-resolution camera.

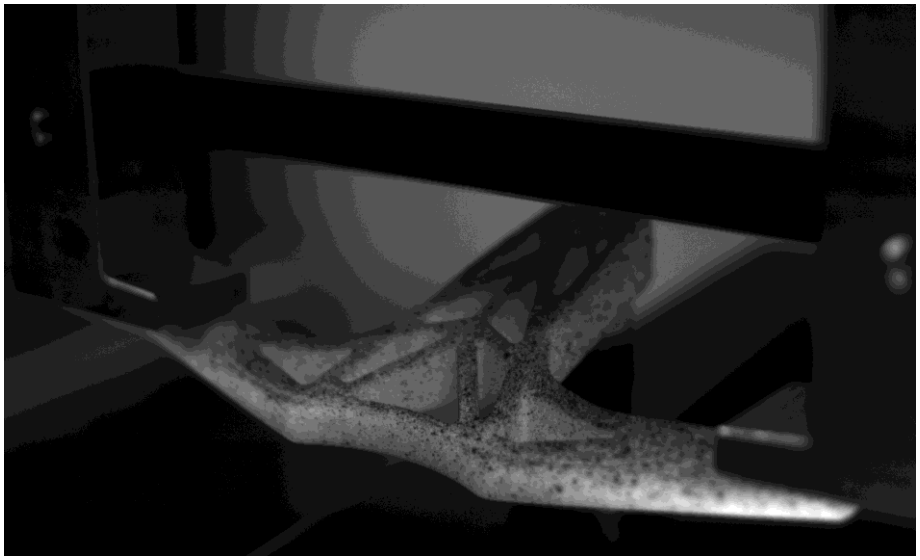

Figure 16 Test setup for bike handle

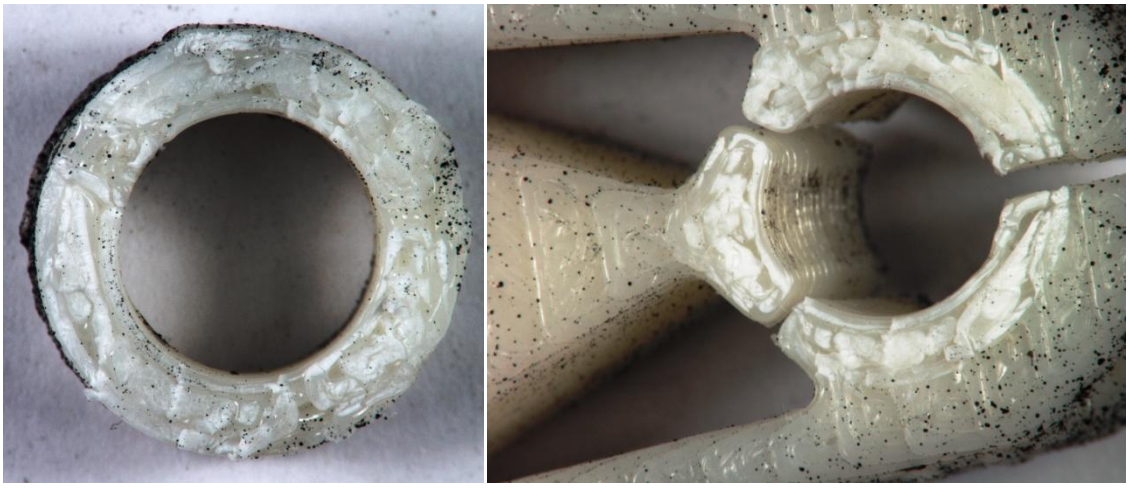

Figure 17 Failure surface of bike handle

The failure surface is at same plane where the protruded part was started to build. Joints are prone to higher stress concentration so such areas are vulnerable too in 3D printed parts as in other structures. Also, the fracture surface shows that there are some defects in the layer and the layer was not perfectly bonded with the adjacent layers. Normally, protruded parts are laid after finishing other parts while building. It gives enough time to cool down the surface from where protruded parts are laid. The bonding between two layers is not same when both layers are hot and liquid compared to the bonding between

one hot semi liquid layer and another cold solid layer. Test result shows the bonding between hot semi liquid layer and cold solid layer is comparatively weak.

5.2.2 DIC Result

Number of images captured	About 22,000
Test Duration	About 440 seconds
Failure occurred at image number	21,956
Number of images taken for strain extraction	24 (After each 1000 starting from zero until failure image)
Force associated in failure	Normal force perpendicular to layer orientation
Maximum strain in X-axis E_{xx}	2.8
Maximum shear strain E_{xy}	0.95
Maximum strain in Y-axis E_{yy}	3.4
Maximum force	132 N

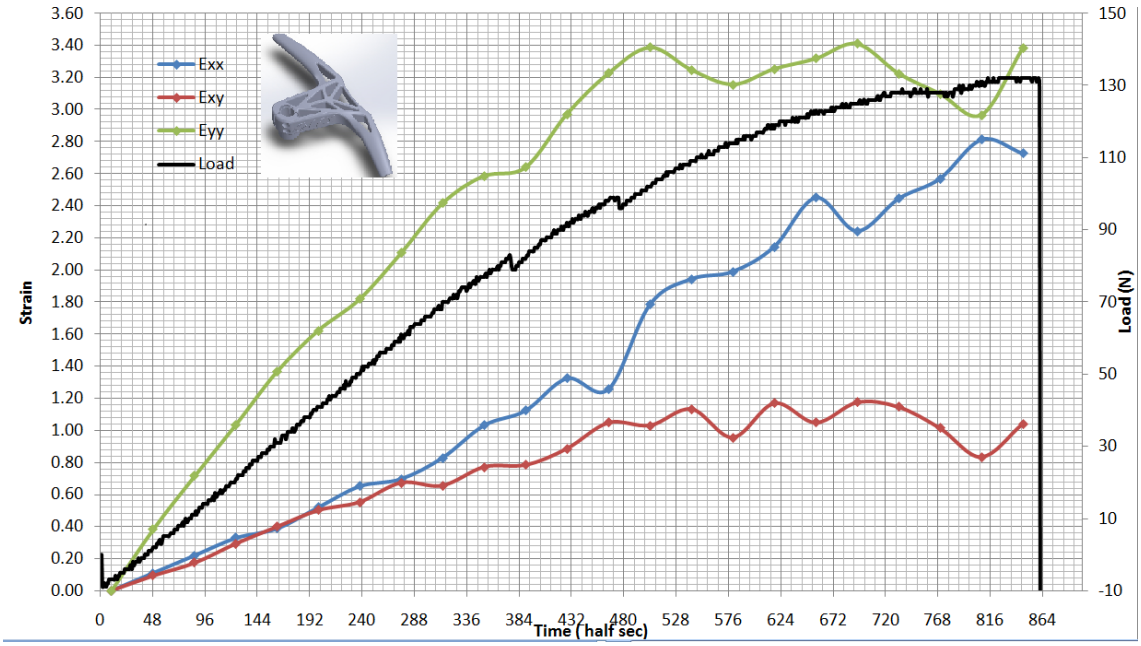

Graph 11 Loading and Strain Curve (bike handle)

Failure point was out of focus in this specimen case, so the strain at the different point of the specimen was studied. Strain at the middle area between two edges of the handle was studied. At the study point, the force was loaded perpendicular to the building

orientation and was causing bending. The load was pushing the two edges downward. It is obvious that the strain is higher in Y-direction, but the bending was also causing the axial displacement resulting higher magnitude of strain in the x-direction. Small fluctuations in the load curve were seen caused by the crack initiation. Multiple cracks were initiated in the study area but eventually failure occurred at a different point as in brittle materials.

5.3 Test Specimen 3 (Nut and Bolt)

3D printed nut and bolt were tested with the normal uniaxial force perpendicular to the building orientation. The speed of the displacement from the test machine was 1mm/min. The result was similar to the bike handle as the head of the bolt splitted from the rest of the part at the same plane where the threaded part started to protrude from its head. The following figure shows the test setup and the failure surface under the high zoom.

5.3.1 Fracture Surface Analysis

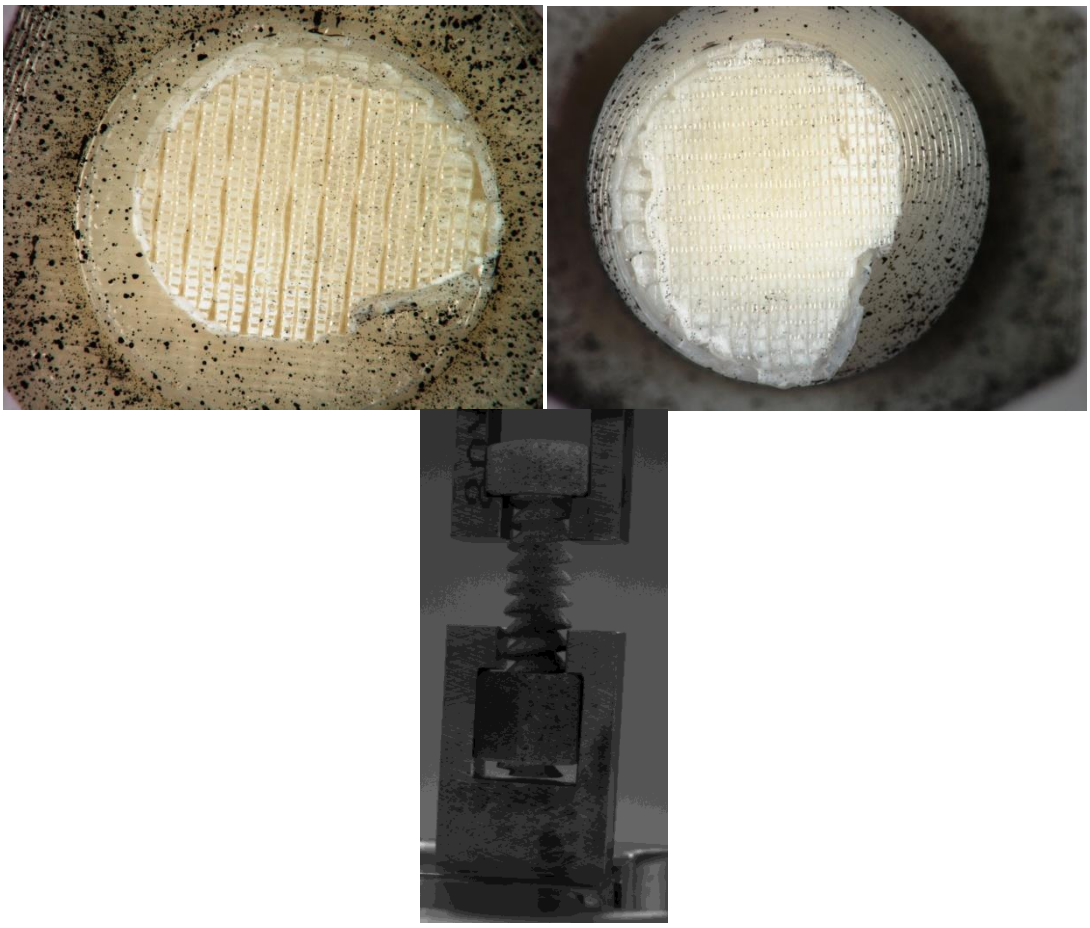

Figure 18 Test set up and fracture surface from nut and bolt

5.3.2 DIC Result

Table 11 Test Summary (Nut and Bolt)

Number of images captured	About 8,700
Test Duration	About 90 seconds
Failure occurred at image number	8,580
Number of images taken for strain extraction	35(After each 250 starting from zero until failure image)
Force associated in failure	Normal force perpendicular to layer orientation
Maximum strain in X-axis E_{xx}	0.024
Maximum shear strain E_{xy}	0.033
Maximum strain in Y-axis E_{yy}	0.16
Maximum force	1275 N

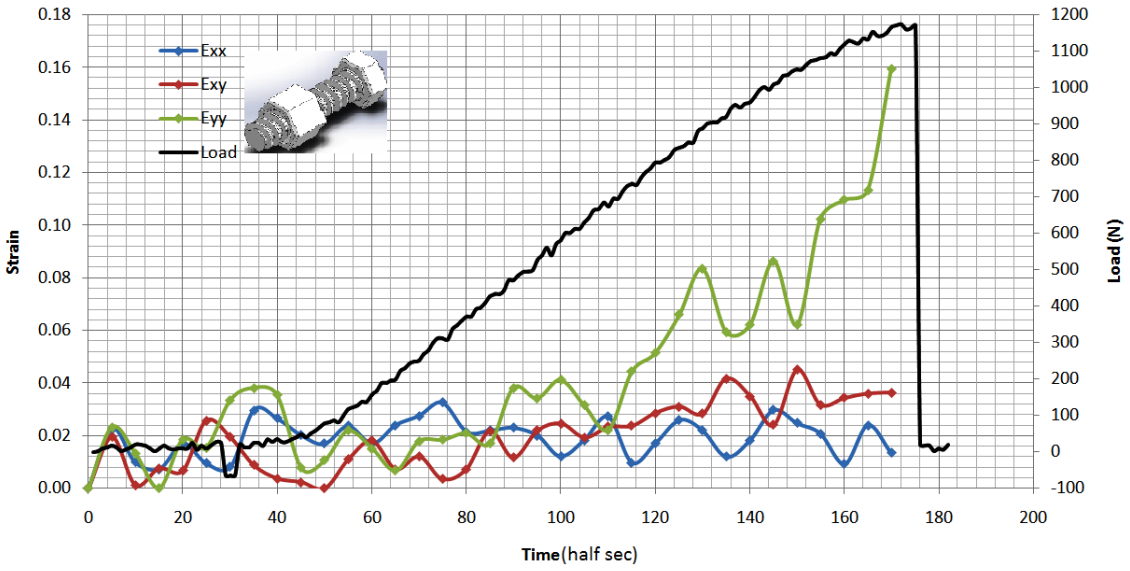

Graph 12 Loading and Strain curves (Nut and Bolt)

This case was very simple in the case of loading and displacement. The tensile force was acting in y-direction perpendicular to the built direction of the specimen. So, the higher magnitude of E_{yy} strain compared to other two strain values is obvious. This specimen provides the insight about the low magnitude of displacement when the normal force acts perpendicular to the built direction although the force is sufficiently high. The displacement was low, and the magnitude of strain in y-direction increased rapidly near the failure. The time between crack initiation and the fracture was just about 5-10

seconds, considering the slower increment in the force. Strain values were very unstable and continuously fluctuating from the starting point due to the nut slipping from the bolt.

5.4 Test Specimen 4 (Chain)

3D printed chain is tested under the normal force that is perpendicular to its build direction. Following set up shows the test setup for the test.

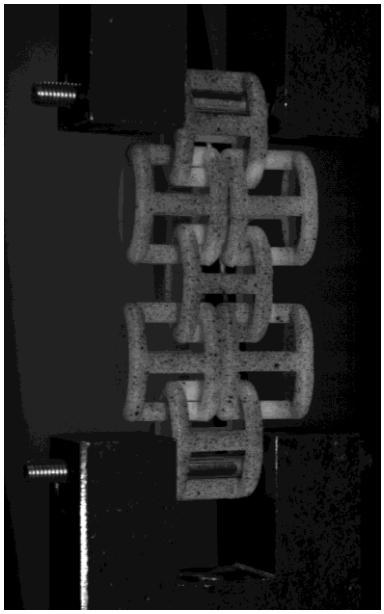

Figure 19 Test set up for the chain

The chain was fixed as shown in the figure above. The top fixture was fixed, and the bottom fixture was moving down slowly at the rate of 2 mm/min creating the normal force on the chain. Chain sustained the load until the breaking happened in no time without showing any sign of crack initiation and propagation.

5.4.1 Fracture Surface Analysis

Figure 20 Failure surface from chain

The fracture surface in the chain is so small that even under the full zoom it does not look so big. It is small but gives enough information to conclude that fracture surface is in the same plane perpendicular to the force applied. Moreover, one of the fracture surfaces also shows that there was a non-negligible defect on that layer which might have triggered the failure to happen at that particular level.

5.4.2 DIC Result

Table 12 Test Summary (Chain)

Number of images captured	About 7500
Test Duration	About 71 seconds
Failure occurred at image number	7,105
Number of images taken for strain extraction	31(After each 250 starting from zero until failure image)
Force associated in failure	Normal force perpendicular to layer orientation
Maximum strain in X-axis E_{xx}	0.05
Maximum shear strain E_{xy}	0.153
Maximum strain in Y-axis E_{yy}	2.1
Maximum force	158 N

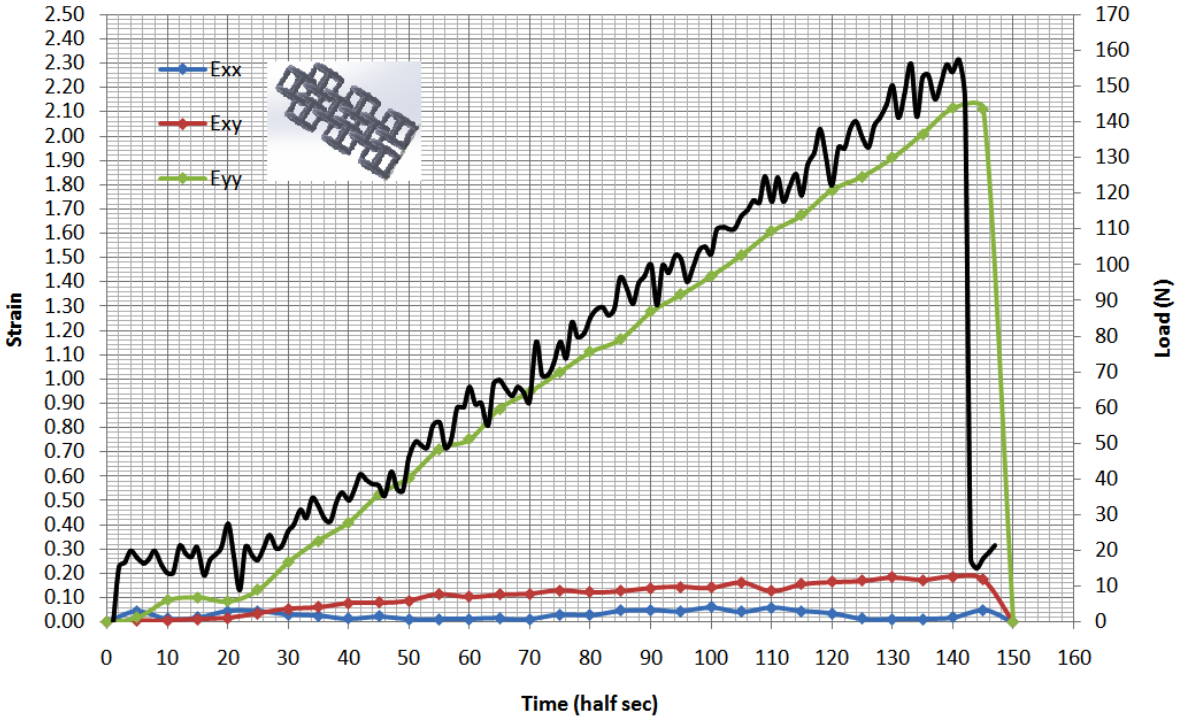

Graph 13 Loading and Strain Curves (Chain)

Test specimen 4, is made by multiple similar parts which have multiple degrees of freedom in a different direction. The normal force was applied from the two ends perpendicular to the building orientation. Force applied and building orientation is similar to that of the test specimen 3, (nut and bolt) and so was the failure result. When graphs are compared to each other, they have different characteristics. Strain curves were fluctuating in the case of nut and bolt and load curve was stable. In this case, load curve is fluctuating, and strain curves are stable. There was no possibility of slipping in this case as the nut was slipping in the previous case. Slipping off the nut caused the fluctuation in strain curves. Many smaller crack formations in the case of the chain might have caused the release of load causing fluctuation in loading curve. The cross-sectional area of the chain is significantly lower than that of nut and bolt. Smaller cross-sectional area increases the possibility of having many smaller crack formations which are not readily visible to naked eyes. Failure strain in test specimen 4(chain) is higher than test specimen 3 (nut and bolt). Slipping does not increase the displacement in the test specimen but crack opening increases the displacement magnitude.

5.5 Test Specimen 5 (Collector)

A rotating part that collects something for example water, when it is in the bottom half of the rotation and releases the material when it is in the upper half of the rotation was 3D printed and tested with the above explained test setup. The collecting points are on

the both ends, and the part is fixed in the middle. The picture below shows the test setup for the part.

Figure 21 Test set up for collector (also shows the failure)

The part has square holes in the middle so that it cannot rotate when the rotating force is applied. It is pulled from one side producing torque and bending movement on the part. Displacement rate of the testing machine was 5mm/min. Building orientation of the part is perpendicular to the force being applied. The crack initiating point is again the high-stress concentration point. Crack does not propagate through the same layer but breaking each adjacent layer one by one. The direction of propagation is almost 45 degrees to the building direction. The experiment was stopped when the crack met the central fixture hole. If the picture is observed clearly, some other layers also develops cracks that-can be seen on either side of the fixation point. The failure has happened due to the combined effect of both shear and normal force. The part was not completely broken into two pieces but to study the failure surface it was broken manually by hands later on.

5.5.1 Fracture Surface Analysis

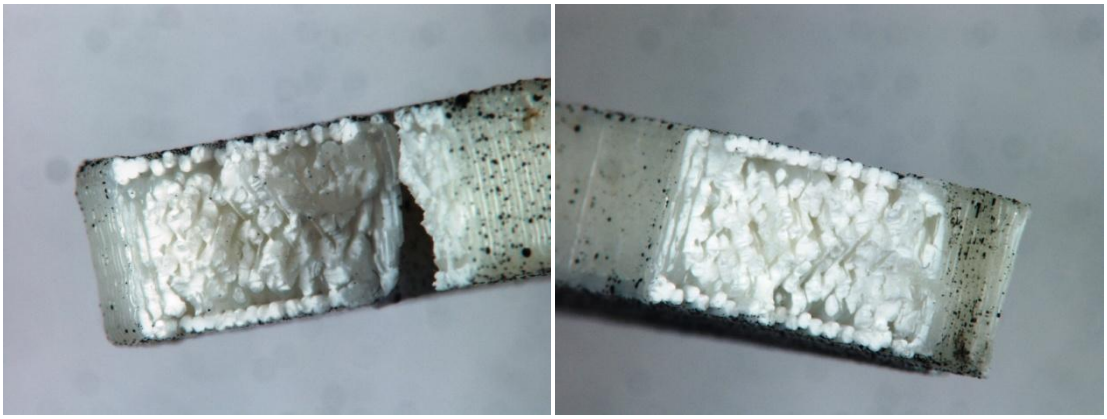

Figure 22 Failure surface from collector

The surface that failed during the experiment has very rough and uneven surface. Some layers were broken due to normal force and some were due to shear force. Also, some bonding defects can also be seen as the failure planes were not seen in perfect touch with each other.

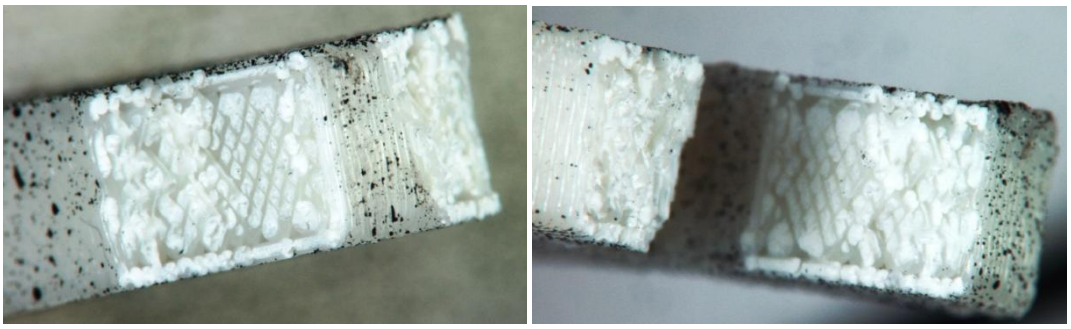

Figure 23 Failure surface from collector (hand)

Just for the rough comparison, the fracture surface formed from manually breaking the parts using hands was also studied. The much obvious difference was on the fracture plane. In the case of hand broken surface, the fracture occurred almost on the straight plane excluding the inbuilt imperfect bonding.

5.5.2 DIC Result

Table 13 Test Summary (Collector)

Number of images captured	About 96,500
Test Duration	About 850 seconds
Failure occurred at image number	96,074
Number of images taken for strain extraction	50(After each 1000 starting from zero until failure image)
Force associated in failure	Both normal force and shear force induced from bending
Maximum strain in X-axis E_{xx}	0.22 (2 points)
Maximum shear strain E_{xy}	1.6
Maximum strain in Y-axis E_{yy}	1.4
Maximum force	73 N

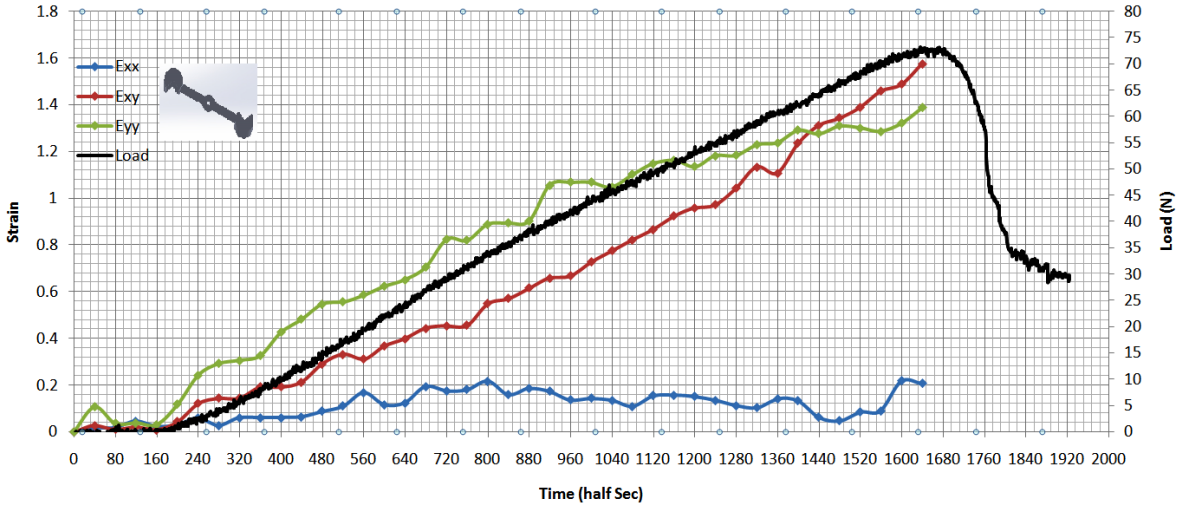

Graph 14 Loading and Strain Curves (Collector)

E_{xy} strain magnitude was higher around the failure area in this specimen along with the E_{yy} strain magnitude. So, both the strain factors played an important role in the failure. The bending force was applied to the specimen that was perpendicular to the building orientation of the specimen. Both E_{yy} and E_{xy} strain parameters were gradually developed with the rising load magnitude. The strain curves have little ups and downs in the curve. It is because of the small slips that occurred at the point where the specimen

was fixed. Also, without failing the whole part, there were enough possibilities of crack initiation in different layers at different point of time.

5.6 Test Specimen 6 (Handle)

The door handle was also 3D printed for testing. The fixture of the door handle was fixed to the plate and pulled up from the middle as it is pulled when attached to the door. The testing machine was applying the force with the displacement rate of 2 mm/min. The crack was developing slowly than it happens in high brittle materials like a mirror and other previous parts. There was a small difference in this specimen and another specimen with protruded part. The protrusion in this part was not totally embedded in another previously laid plane. Protruded part and the previously built layer has the same edge on one side, and the another edge was slightly rounded unlike in other parts. Another reason behind this might be because the protruded part was not laid on the plane which has already been cooled to some extent. Failure mostly occurred due to the normal stress induced due to the bending of the part as it was pulled up.

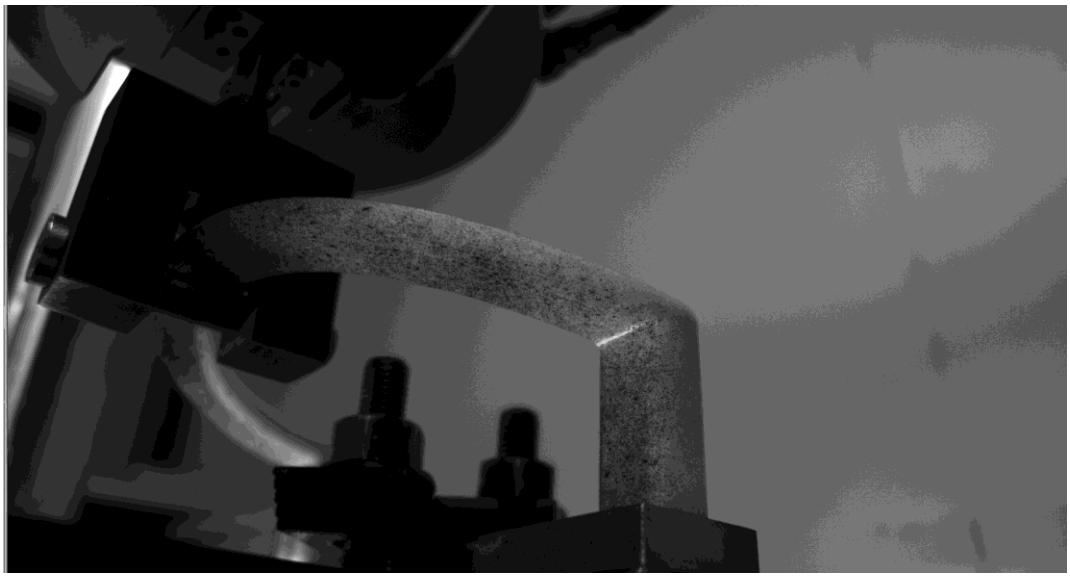

Figure 24 Crack occurring in the door handle while testing

5.6.1 Fracture Surface Analysis

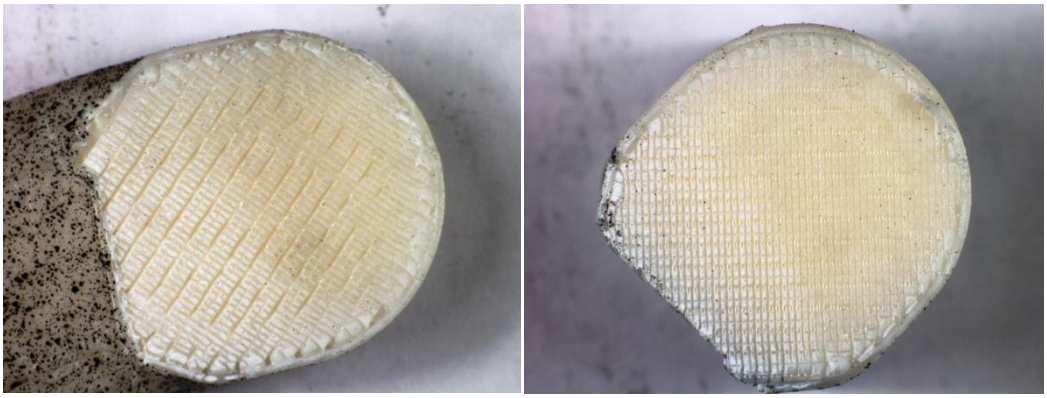

Figure 25 Fracture surface from door handle

Fracture surface of the door handle was not much different from other protruded part failure, but the initiation of the crack was much slower. A higher magnitude of the radius at the joint would have made the failure more interesting. Fracture happened in the same joint plane from where the protruded part started to be built.

5.6.2 DIC Result

Table 14 Test Summary (Handle)

Number of images captured	About 50,100
Test Duration	About 950 seconds
Failure occurred at image number	50,025
Number of images taken for strain extraction	27 (After each 1000 starting from zero until failure image)
Force associated in failure	Normal force and shear force induced from bending
Maximum strain in X-axis E_{xx}	0.2
Maximum shear strain E_{xy}	3.6
Maximum strain in Y-axis E_{yy}	15.5
Maximum force	0.31 KN

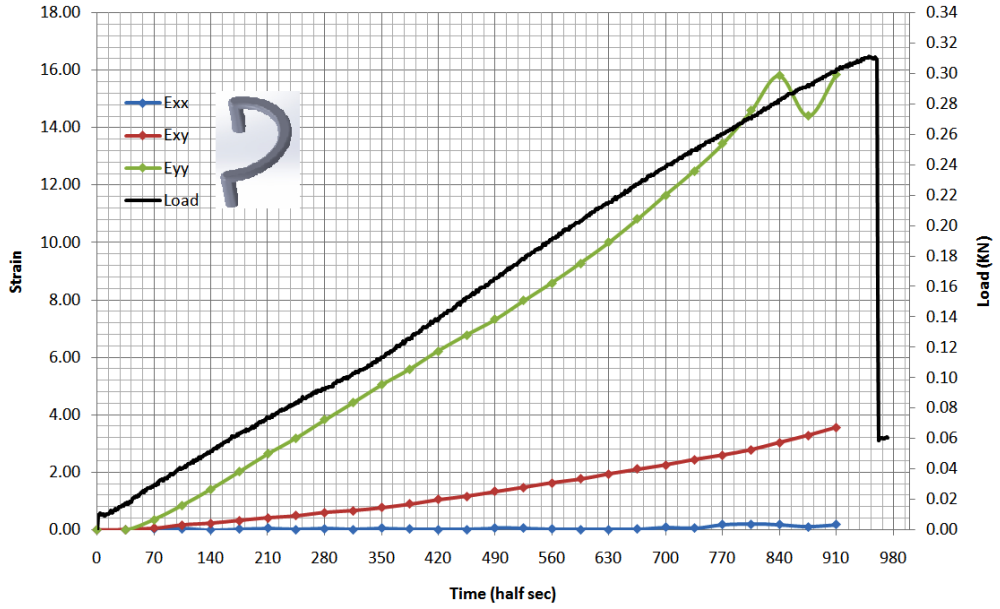

Graph 15 Loading and Strain Curves (Door handle)

This specimen had high deformation case, mostly because of the region that was bending. The length of the part was longer in this case. The part was being pulled upward i.e. in y-direction. The region that was bending was attached at the point where the failure occurred. Both the strain curves are developing in the proportional amount of the force applied. The strain was higher mainly due to deformation or bending rather than displacement. The amount of force required was not so high because the part failed because of bending moment rather than force directly.

5.7 Test Specimen 7 (Hinge)

Hinges that are attached to the doors and windows are 3D printed in one assembly and tested for the fracture surface and strain analysis. The normal force was applied at the joints pulling two major parts that are attached to the door and door frame. Only, normal force was applied but the geometry of the joint was very complex to figure out what was the type of the acting force on the joint. The displacement rate of the load being applied was 2 mm/min.

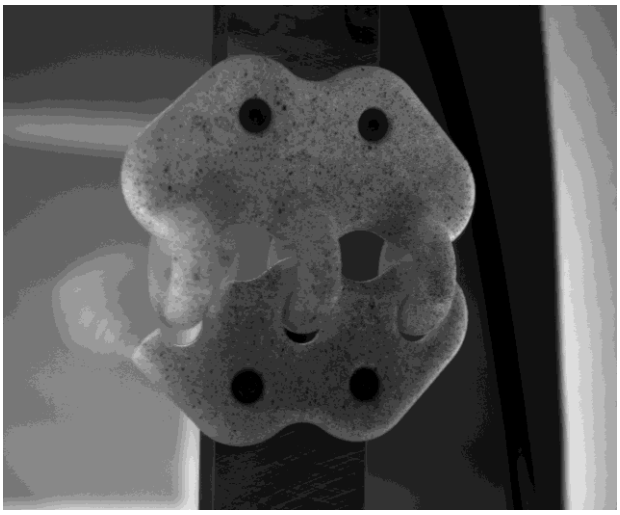

Figure 26 Test set up for hinge and broken piece chipping away

5.7.1 Fracture Surface Analysis

The single piece turned into three pieces, one big and two smaller pieces. It created three pairs of fracture surfaces. Specimen resisted the load for a longer time, but both fracture happened in quick succession that it was hard to tell which piece broke first, so all six fracture surfaces were studied.

Figure 27 Fracture surface 1 from hinge

The picture shows the fracture surfaces from the main part and its respective surface from two different pieces. The building orientation was so complex that it is hard to tell

what force was acting dominantly on the fracture point. The force was neither parallel nor perpendicular to building orientation. Fracture surface has uneven and rough surface. The fracture happened due to combined resultant of shear force and normal force and created the uneven fracture surfaces. Similarly, the following picture shows the fracture point where the above two pieces (not the major piece) separated from each other. They separated exactly at the point where the applied force acted like a total shear force on that point. From the observation in previous cases, the crack and failure might have happened at the following fracture place first. Then to make the way out, above two fractures happened simultaneously or in short succession.

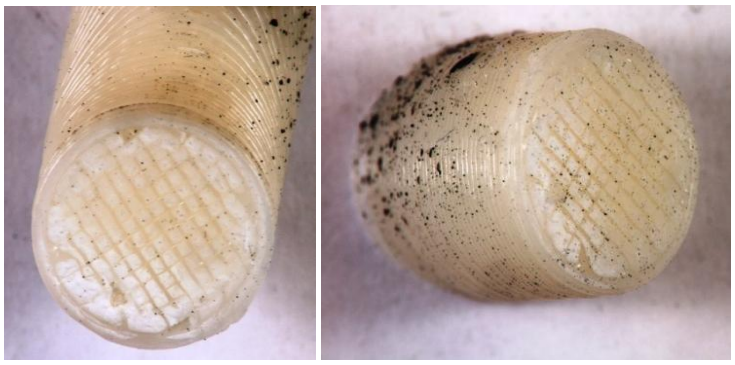

Figure 28 Fracture surface 2 from hinge

5.7.2 DIC Result

Table 15 Test Summary (Hinge)

Number of images captured	About 24,500
Test Duration	About 240 seconds
Failure occurred at image number	23,926
Number of images taken for strain extraction	26(After each 1000 starting from zero until failure image)
Force associated in failure	the normal force with varying angle with layer orientation
Maximum strain in X-axis E_{xx}	0.76
Maximum shear strain E_{xy}	1.6
Maximum strain in Y-axis E_{yy}	2
Maximum force	4.1 KN

The failure point of the specimen was very complex as the specimen was round at the failure point. Building orientation was not same along the line of action of the force.

The fracture pieces for this specimen were three. The graph shows a small drop in the loading sequence. The weakest bond between the two layers failed at that moment creating the crack but because of the structure the force could not be released totally. Eventually, it went to break the specimen at other two places making it three. Also from the table, all the strain values are comparable to each other and seem to have enough influence on the failure.

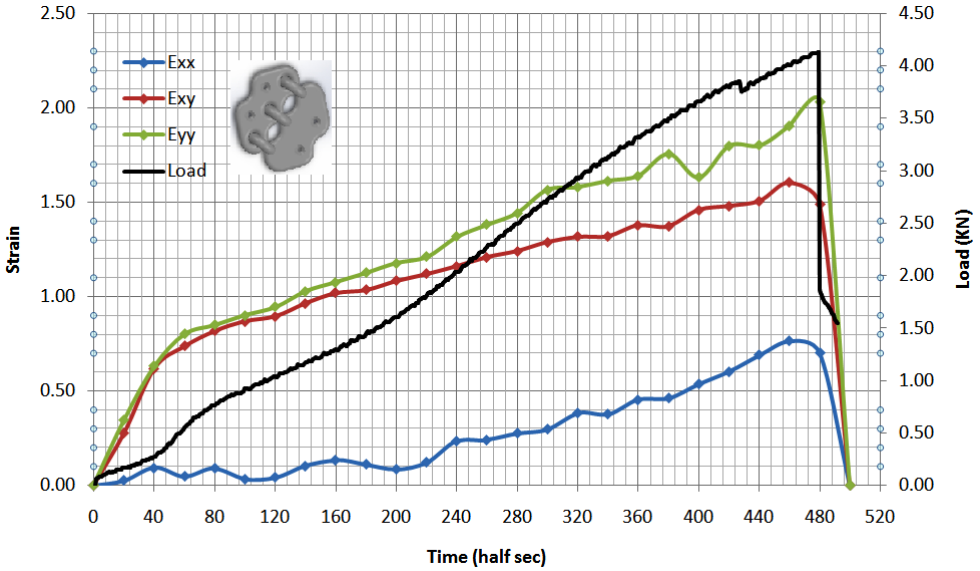

Graph 16 Loading and Strain Curves (Hinge)

All the strain curves are rising gradually with the increasing force showing that all the strains played some role in the fracture surfaces. Particularly, shear strain and strain at y-direction were increasing at a different rate from 0 until 60 half seconds and then the rate changed dramatically after that. Fracture surface well explains the phenomenon occurring at the point. That could be the point where the first fracture surface has happened.

5.8 Test Specimen 8 (Valve)

The head of the steering valve (without its shaft) which is commonly used in water supply and taps was 3D printed and tested, similar to other test specimens. This specimen was little tricky to mimic the real condition to apply the torsion like force. The best way possible was adopted to mimic the real life scenario. Valve has square holes in the middle that goes in the square rod. The square shape matching prevents its rotation. The following figure shows the test setup for the specimen.

Figure 29 Test set up for valve and failure occurring while testing

The rod that goes through under the arm of the valve is pulled up to apply the rotating force on the specimen. It was pulled up at the rate of 2mm/min displacement. The arm was built in the curved orientation at those points where arms were joined at the circumference of the round structure. Failure image from the test is alone enough to tell about the crack formation in multiple places. Ultimately it failed at the arm that was directly under the influence of the loading arm. Also, some layers were still seen connected to both major piece and fractured piece. The arm was broken and separated from the major piece manually to study the fracture surface.

5.8.1 Fracture Surface Analysis

Figure 30 Fracture surface from valve

When the layer orientation and applied force are not parallel or perpendicular, fracture occurs due to the effect of combined loading of both normal and shear force. Fracture surface is not on the same plane. Few layers were also seen still connected with both

fractured pieces signifies that the layers were broken at different instant of time which means the crack was propagating slowly. Whenever the failure occurs between the layers, the specimen behaves less brittle.

5.8.2 DIC Result

Table 16 Test Summary (Valve)

Number of images captured	About 10,000
Test Duration	About 205 seconds
Failure occurred at image number	9,996
Number of images taken for strain extraction	23(After each 500 starting from zero until failure image)
Force associated in failure	Both normal force and shear force induced from torque
Maximum strain in X-axis E_{xx}	2.5
Maximum shear strain E_{xy}	0.8
Maximum strain in Y-axis E_{yy}	3.15
Maximum force	255 N

A higher magnitude of the load was not required to observe the failure happening. The building orientation was not straight at the failure point. The rectangular part was connected to the rounded part. The curved building orientation transferred the applied load, so the displacement was occurring in all direction.

All three strain curves were gradually rising with the increasing force creating displacement in all directions. Fluctuation in curves around the failure time is obvious from the fracture surface results. There were multiple points where larger cracks were opened up. Test specimen continued to resist the load despite having larger failure cracks at different points in the specimen. Although there were multiple bigger cracks opening but the specimen was still intact as a single piece which caused the decreasing and increasing magnitude of load and strains towards the end points. Graph 17 shows the loading curve and strain curves.

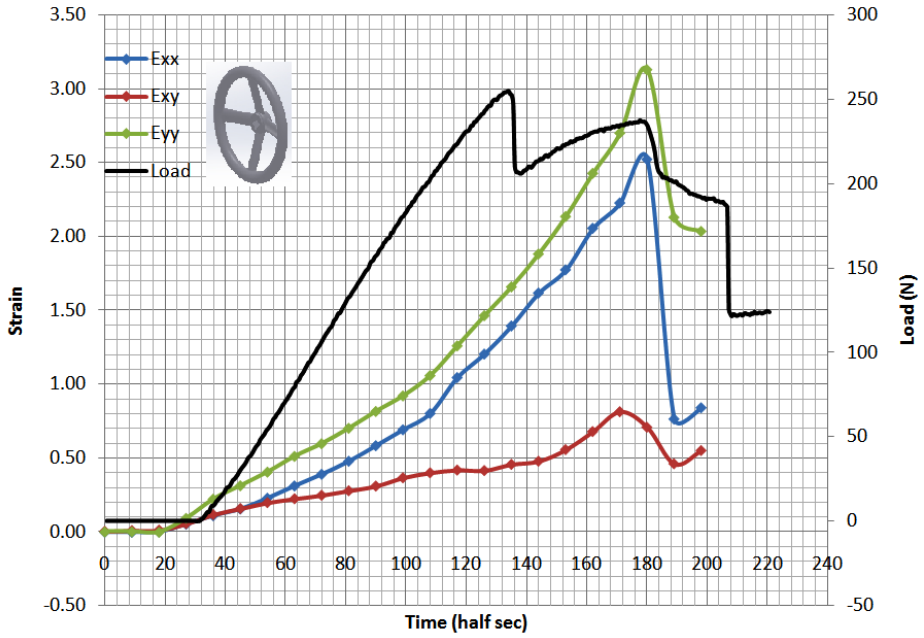

Graph 17 Loading and Strain Curves (Valve)

5.9 Test Specimen 9 (Wrench)

The last specimen that was tested was wrench that is used to open nuts and bolts. The nut of the same size as the wrench was fixed on a rod restricting it to rotate, and the wrench was fixed on the nut. Force was applied slowly mimicking the nut opening condition from another end. The following picture shows more information about the test setup.

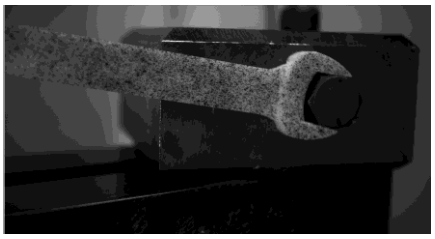

Figure 31 Test set up for the wrench

As shown in the figure, one end was hooked to the bolt head, and from another end, the force was being applied at the rate of 5 mm/min displacement. Eventually, the wrench slipped away from the nut and test setup. When the wrench was used later manually to tighten the nut, fractured occurred. Fracture surface occurred due to accidental breaking was also studied which showed the fracture happened at the same layer where the applied force was normal and perpendicular to it.

5.9.1 Fracture Surface Analysis

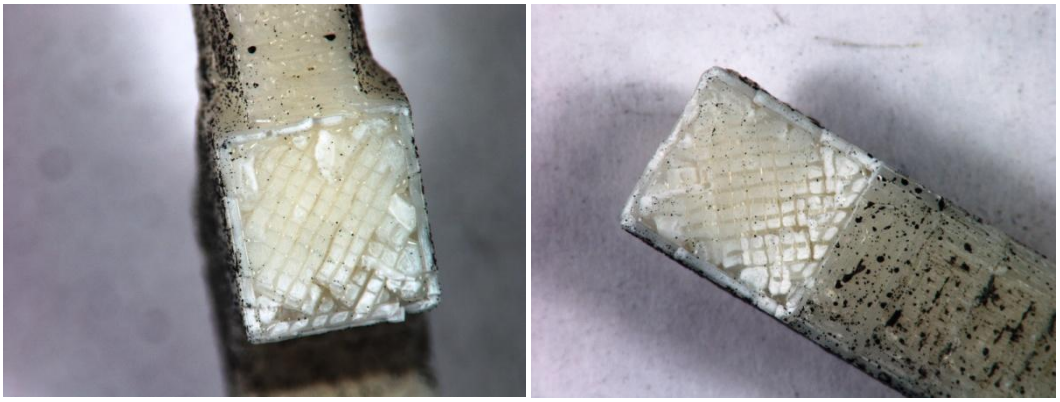

Figure 32 Fracture Surface (Wrench)

The fracture occurred at the plane which is parallel to the applied force. Shear force induced from the bending broke the specimen. Results look similar to other test specimens that have been broken by a shear force parallel to the layer orientation.

5.9.2 DIC Result

Table 17 Test Summary (Wrench)

Number of images captured	About 26,000
Test Duration	About 150 seconds
Failure occurred at image number	25,868
Maximum strain in X-axis E_{xx}	0.05
Maximum shear strain E_{xy}	0.2/0.025
Maximum strain in Y-axis E_{yy}	0.48/0.46
Maximum force	4 N

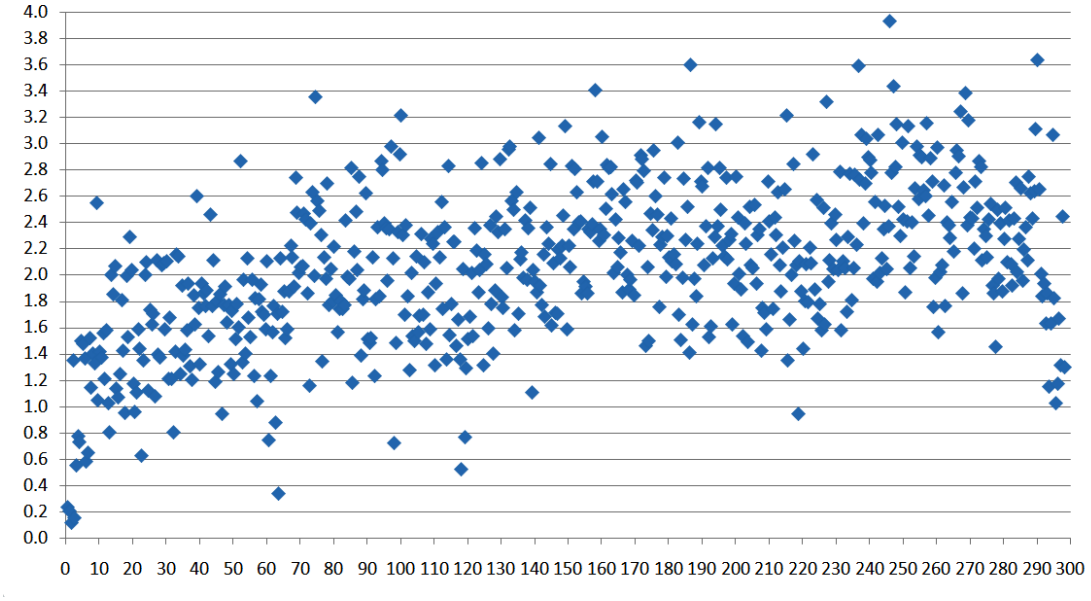

Graph 18 Loading Sequence (Wrench)

This specimen was constantly slipping from its fixation point and rotating slowly with the increasing force. Hence the maximum force recorded was 4 N which was unable to create the proper strain curves.

6 Discussion and Conclusion

As concluded from the theoretical analysis, some approach needs to be started towards building new theory to calculate and predict the failure in 3D printed parts. This research was continued from theoretical analysis to produce some results for foundation or basic work towards new theory. One step was taken back from where other researches started their studies about the strength of the 3D printed parts. Some experiments were carried out to understand more about the strain behavior, displacement, failure mechanism and strength in 3D printed parts.

The fracture in different layer orientation causes different types of fracture surfaces which were seen from the comparison of the fracture surface of gear tooth in different layer orientation. The fracture surfaces in all test specimens showed the defects or imperfections in the layer that surely decreases the strength of the parts. However, there were not enough evidence observed which proved those defects can alter the failing layer in 3D printed parts. The cure to those defects will surely strengthen the 3D printed products though. Despite imperfections in layers built, failure mostly originated from the similar couple of cases which can be outlined as below.

- When the applied force is shear and the layer orientation is parallel to it.
- When the applied force is normal, and the layer orientation is perpendicular to it.
- On the plane where the protruded parts are laid on the previously laid plan.

- At the joint of two different types of layer orientation.

Strain-load curves also generated some evidence to make some important conclusions. Strains in most cases of 3D printed parts are very low, and failure happens close to that of brittle materials. The weakest bond in 3D printed parts is between the layers whose bond plane is perpendicular to the normal force. The failure on those layers happen most frequently and is similar to brittle material. It is the reason behind the 3D printed parts failing like brittle materials. If the failure happens in other layers then the strain magnitude is high. So, building orientation always plays an important role in failure. It is seen clearly from the varying strain values with varying layer orientation and force types. Fluctuations in load curve in some test specimen cases shows that some phenomena occur during the failure that releases the load applied. One of them is certainly crack initiation between different layers and different instant of time. There could be other reasons too which still need more detailed research. Strain magnitude is lower than other materials or structures, but the behavior of the strain was not totally absurd or unique than other materials or structures. For instance, if similar 3D printed parts and parts manufactured from other processes are tested under same loading and test conditions, there might be difference in strain magnitude, but the same strain parameter will be responsible for the failure.

7 Future Proceedings

There are still lots of work that should be done to increase the accuracy in the strength modeling of the 3D printed parts. There are already some limitations in this research work which should be eliminated in the future research to produce more accurate strength prediction and failure mechanism results for 3D printed parts. This research mostly focused on creating the base work to continue the research in the field, so a wide variety of test specimen were tested and analyzed. Sticking to one standard test specimen and varying different parameters which has effect on the strength and failure condition observed during this research will help to reduce more strong conclusions. The complex geometry of the test specimen posed the major challenge in analyzing the experimental results in this research. It barred to calculate the cross-sectional area of the specimen. Experimentation of the specimen which has an easier cross-sectional area to calculate would allow the result to analyze the result, independent of the size of the specimen. Hence, the outcomes of the result can be broadened.

Also, there are few other areas where the research has left untouched. The effect of the recurring loads on the 3D printed parts is another good area of research as a continuation of this research work. Fatigue and fracture analysis of the 3D printed part is appealing strongly to continue work in this study area. There are various parameters that affect the strength of 3D printed parts as discussed in the literature review section of this research. In this research only dominant parameter i.e. building orientation is considered. There is also the possibility of the further research to include all those parameters in the strength prediction formulation. It sounds challenging, but more research and attempt can produce positive results.

There is never an end to the research work in any field, and this is just the beginning and small part of the research in strength and failure mechanism for 3D printed parts. The author is hopeful that the outcome of this research will provide as the base work for the future studies.

8 References

[1] Anisotropic material properties of fused deposition modeling ABS Ahn, Sung-Hoon;Montero, Michael;Odell, Dan;Roundy, Shad;Wright, Paul K *Rapid Prototyping Journal;* 2002

[2] Croccolo, Dario, Massimiliano De Agostinis, and Giorgio Olmi. "Experimental characterization and analytical modeling of the mechanical behavior of fused deposition processed parts made of ABS-M30." *Computational Materials Science* 79 (2013): 506-518.

[3] Gibson, Ian, David W. Rosen, and Brent Stucker. *Additive manufacturing technologies*. New York: Springer, 2010.

[4] Fodran, Eric, Martin Koch, and Unny Menon. "Mechanical and dimensional characteristics of fused deposition modeling build styles." *Solid Freeform Fabrication Proc*. 1996.

[5] Hossain, Mohammad Shojib, et al. "Improved Mechanical Properties of Fused Deposition Modeling-Manufactured Parts Through Build Parameter Modifications." *Journal of Manufacturing Science and Engineering* 136.6 (2014): 061002.

[6] Sayre III, Robert. *A Comparative Finite Element Stress Analysis of Isotropic and Fusion Deposited 3D Printed Polymer*. Diss. Rensselaer Polytechnic Institute, 2014.

[7] Strength Theories of lamina [https://nanoed.tul.cz/pluginfile.php/3604/mod_resource/content/1/Strength-theories-of-lamina.pdf] Accessed on 23.08.2015

[8] Caulfield, B., P. E. McHugh, and S. Lohfeld. "Dependence of mechanical properties of polyamide components on build parameters in the SLS process." *Journal of Materials Processing Technology* 182.1 (2007): 477-488.

[9] Thomas, James P., and John E. Renaud. "Design of Fused-Deposition ABS Components for Stiffness and Strength." (2003).

[10] Es-Said, O. S., J. Foyos, R. Noorani, M. Mendelson, R. Marloth, and B. A. Pregger. "Effect of layer orientation on mechanical properties of rapid prototyped samples." *Materials and Manufacturing Processes* 15, no. 1 (2000): 107-122.

[11] Perez, Angel R. Torrado, David A. Roberson, and Ryan B. Wicker. "Fracture surface analysis of 3D-printed tensile specimens of novel ABS-based materials." *Journal of Failure Analysis and Prevention* 14.3 (2014): 343-353.

[12] Ziemian, Constance, Mala Sharma, and Sophia Ziemian. *Anisotropic mechanical properties of ABS parts fabricated by fused deposition modelling*. INTECH Open Access Publisher, 2012.

[13] Caulfield, B., P. E. McHugh, and S. Lohfeld. "Dependence of mechanical properties of polyamide components on build parameters in the SLS process." *Journal of Materials Processing Technology* 182.1 (2007): 477-488.

[14] Tymrak, B. M., M. Kreiger, and J. M. Pearce. "Mechanical properties of components fabricated with open-source 3-D printers under realistic environmental conditions." *Materials & Design* 58 (2014): 242-246.

[15] Stava, Ondrej, et al. "Stress relief: improving structural strength of 3D printable objects." *ACM Transactions on Graphics (TOG)* 31.4 (2012): 48.

[16] Farzadi, Arghavan, et al. "Effect of layer printing delay on mechanical properties and dimensional accuracy of 3D printed porous prototypes in bone tissue engineering." *Ceramics International* 41.7 (2015): 8320-8330.

[17] Bagsik, A., and V. Schöppner. "Mechanical properties of fused deposition modeling parts manufactured with Ultem* 9085." *Proceedings of ANTEC*. Vol. 2011. 2011.

[18] http://www.stratasys.com/materials/fdm/absplus Accessed on 06.11.2016

[19] http://teststandard.com/data_sheets/ABS_Data_sheet.pdf Accessed on 20.05.2016

[20] Single Lamina Theory http://link.springer.com/chapter/10.1007%2F3-540-27710-2_10#page-1Accessed on 23.08.2016

[21] Failure criterion eBook Advanced mechanics of material Boresi & Schmidt http://onlinelibrary.wiley.com/doi/10.1002/pc.10671/epdf

[22] http://www.dtic.mil/dtic/tr/fulltext/u2/a144274.pdf accessed on 15.12.2015

[23] Hahn, Hong T., and Stephen W. Tsai. *Introduction to composite materials*. Vol. 1. CRC Press, 1980.

[24] http://ntrs.nasa.gov/archive/nasa/casi.ntrs.nasa.gov/19890005099.pdf accessed on 16.09.2016

[25] Modelling the strength of 3 D Printed parts. Johnny Wikström https://aaltodoc.aalto.fi/handle/123456789/18112 accessed on 16.09.2016

[26] Nahas, Mahmoud N. "Survey of failure and post-failure theories of laminated fiber-renforced composites." *Journal of Composites, Technology and Research* 8.4 (1986): 138-153.

[27] http://www.wmberg.com/catalog/pdf/b00k2-16.pdf accessed on 26.04.2016

[28] McCormick, Nick, and Jerry Lord. "Digital image correlation." *Materials today*13.12 (2010): 52-54.

[29] Abanto-Bueno, Jorge, and John Lambros. "Investigation of crack growth in functionally graded materials using digital image correlation." *Engineering Fracture Mechanics* 69.14 (2002): 1695-1711.

[30] Lecompte, D., et al. "Quality assessment of speckle patterns for digital image correlation." *Optics and lasers in Engineering* 44.11 (2006): 1132-1145.

[31] Verhulp, Eelco, Bert van Rietbergen, and Rik Huiskes. "A three-dimensional digital image correlation technique for strain measurements in microstructures." *Journal of biomechanics* 37.9 (2004): 1313-1320.

[32] Lu, H., and P. D. Cary. "Deformation measurements by digital image correlation: implementation of a second-order displacement gradient."*Experimental mechanics* 40.4 (2000): 393-400.

[33] Pan, Bing. "Recent progress in digital image correlation." *Experimental Mechanics* 51.7 (2011): 1223-1235.

[34] Sutton, Michael A., Jean Jose Orteu, and Hubert Schreier. *Image correlation for shape, motion and deformation measurements: basic concepts, theory and applications*. Springer Science & Business Media, 2009.

[35] Li, Zeyu, and Jinling Wang. "Least squares image matching: A comparison of the performance of robust estimators." *ISPRS Annals of the Photogrammetry, Remote Sensing and Spatial Information Sciences* 2.1 (2014): 37.

[36] Gruen, Armin. "Development and status of image matching in photogrammetry." *The Photogrammetric Record* 27.137 (2012): 36-57.

[37] https://melab.wikischolars.columbia.edu/file/view/AN525+-+Speckle+Pattern+Fundamentals.pdf Accessed on 27/09/2016